THESIS REPORT

Master's Degree

Systematic Design of Gearless Differentials and Analysis of a Potential Mechanism

by B. Madhavan
Advisor: L.W. Tsai

M.S. 96 -7

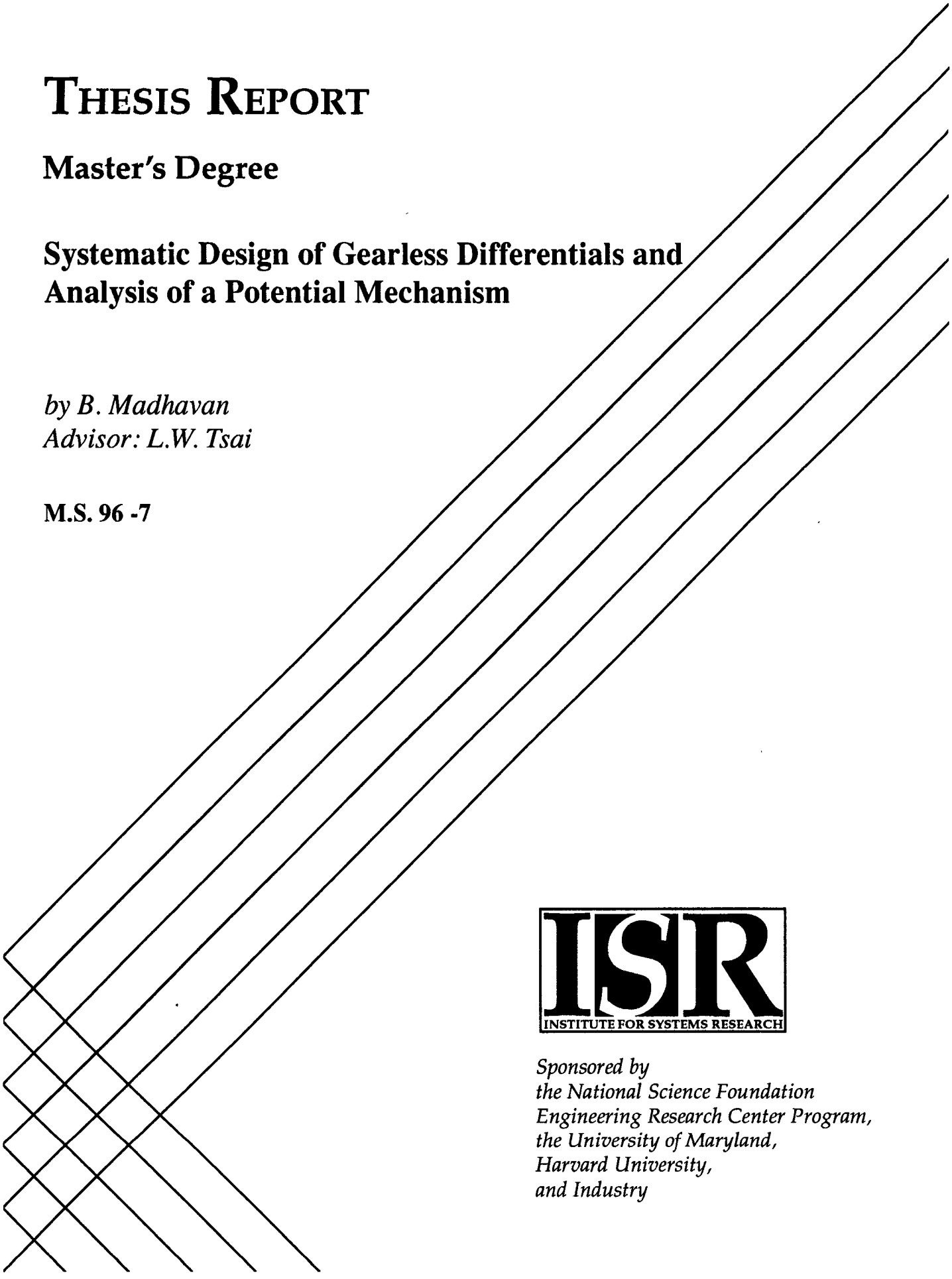

Sponsored by
the National Science Foundation
Engineering Research Center Program,
the University of Maryland,
Harvard University,
and Industry

Abstract

Title of Thesis: Systematic Design of Gearless Differentials and Analysis of a Potential Mechanism

Name of degree candidate: Bharath Madhavan

Degree and year: Master of Science, 1996

Thesis directed by: Professor Lung Wen Tsai
Department of Mechanical Engineering

The method of classification of mechanisms according to kinematic structure and function is used to systematically enumerate gearless differential mechanisms. The method adopted here is to first enumerate 1:-1 constant-velocity shaft couplings which are later transformed into gearless differentials. Preliminary screening of the enumerated mechanisms resulted in four potential 1:-1 constant-velocity shaft couplings that are free from singular conditions. With a little modification, these mechanisms are then converted to gearless differentials. A promising candidate mechanism is chosen and kinematic and dynamic analyses are performed. The dynamic analysis is done using the software package DADS. It is shown that the proposed mechanism does have the potential for use as a gearless differential. Finally design rules are laid out which can be used for the design of an optimal gearless differential.

Systematic Design of Gearless Differentials and Analysis of a Potential Mechanism

by

Bharath Madhavan

Thesis submitted to the Faculty of the Graduate School
of The University of Maryland in partial fulfillment
of the requirements for the degree of
Master of Science
1996

Advisory Committee:

Professor Lung Wen Tsai, Chairman/Advisor
Professor Shapour Azarm
Professor Bruce S. Berger

Dedication

To Mother Nature

Acknowledgements

The work presented here would not have been possible without the guidance of my advisor Dr. Lung Wen Tsai, whose knowledge, expertise, enthusiasm and teaching ability were invaluable. I would like to first thank him for his support and encouragement as well as technical guidance during this work.

I owe gratitude to the Institute for Systems Research for providing me with all the facilities needed to complete this work.

I owe special thanks to Mr. Prasad Dharmasena for installing the package DADS in one of our Sun SPARCs which was used extensively in this work.

I would also like to thank the committee members, Dr. Shapour Azarm and Dr. Bruce S. Berger, for serving on my thesis committee.

Table of Contents

List of Tables

List of Figures

Chapter 1

Introduction

The creation of mechanisms to achieve a given function, which is the conceptual design phase, is perhaps the most difficult phase of mechanical design. The classification of mechanisms according to kinematic structure and function has been a useful aid in the creation of mechanisms. During the mid nineteen-sixties, it has been shown that kinematic structure can be represented by graphs and graphs can be enumerated systematically using the theory of graphs and combinatorial analysis (Dobrjanskyj and Freudenstein, 1967). This is a powerful tool for the creation of mechanisms in a relatively simple but systematic manner. The basic idea underlying this method is the separation of structure from function (Freudenstein and Maki, 1979, 1983, 1984). This is shown schematically in Table 1.1. The method uses the structural characteristics to first enumerate all possible mechanisms within a set of search specifications. Later, the functional requirements are used to screen out infeasible mechanisms. After this initial screening, we end up with some potential mechanisms on which detailed analysis can be done.

Table 1.1: Systematic design of mechanisms (Method 1)

(a) *Structure*

1. Determine freedom, number of moving members, complexity (L_{ind}) and the nature of motion (plane, $\lambda = 3$; spatial, $\lambda = 6$).
2. Find structures of kinematic chains from atlas.
3. Label structures according to types of joints and choice of fixed link in as many different ways as possible.
4. For each structure, sketch corresponding mechanism.

(b) *Function*

Determine the functional requirements for the desired mechanism and the relationship to kinematic structure.

(c) *Structure and Function*

Use functional requirements to screen out unacceptable mechanisms. Remaining mechanisms represent potential solutions and can then be evaluated in greater detail.

1.1 Systematic Design of Mechanisms

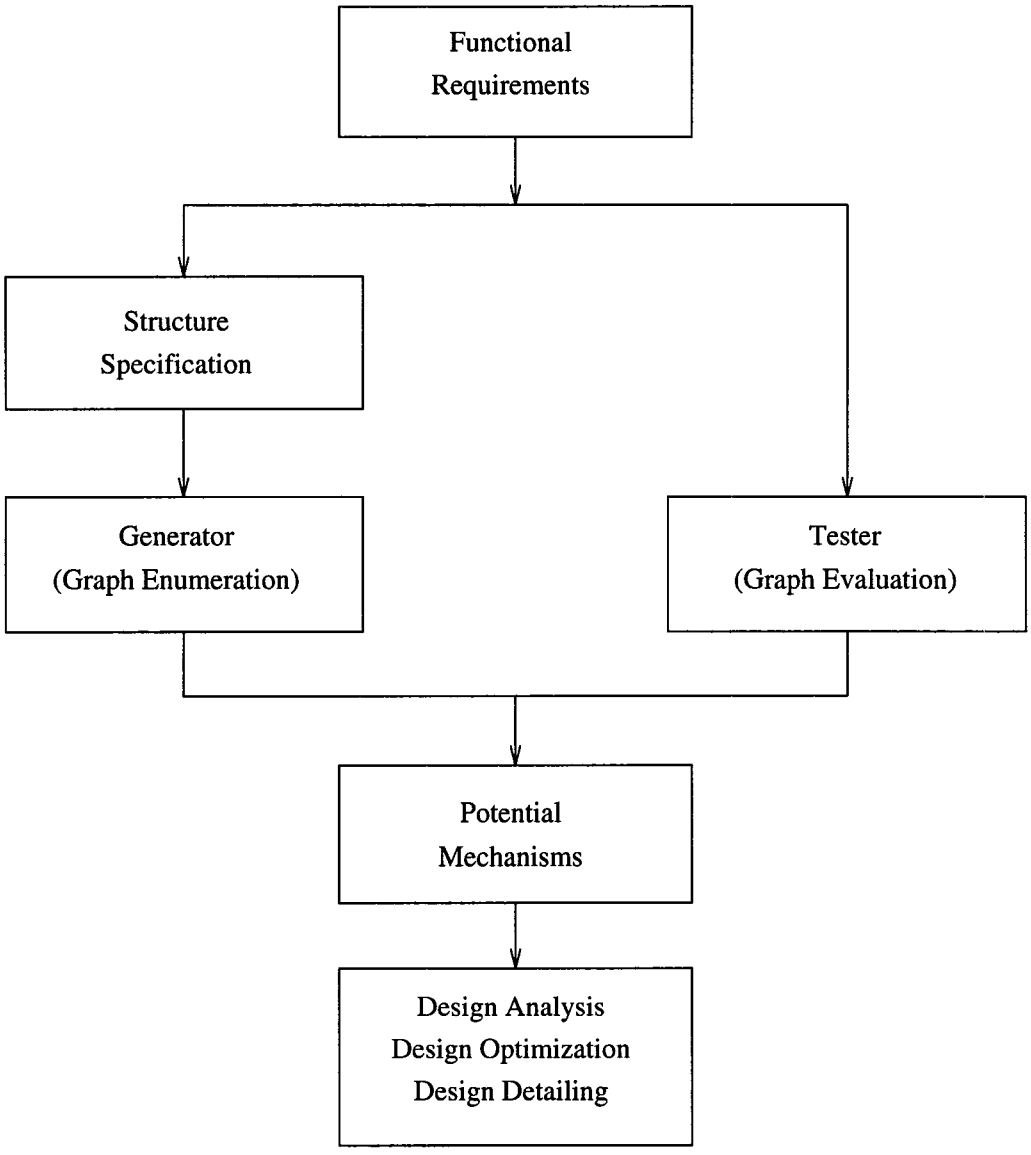

Figure 1.1: Systematic design methodology (Method 2)

Traditionally, the design of a mechanism was achieved by the designer's intuition and ingenuity. However, this approach has a problem. It does not guarantee that all the potential mechanisms, which would have satisfied the functional requirements, have been identified and the best candidate mechanism has been

selected. Later, in the early seventies, more efforts were undertaken to overcome this drawback by developing systematic methodologies for the design of mechanisms. Table 1.1 shows one such method that has been adopted widely for the systematic design of mechanisms.

In this study, a modified approach is used as shown in Figure 1.1 (Chatterjee and Tsai, 1994a and 1994b). In this approach, the functional requirements of the mechanism to be designed are initially laid out. These are very simple requirements that a mechanism should satisfy in order to perform the necessary function. Then, some of the functional requirements of the mechanism are translated into structural characteristics, and incorporated in a "Generator" for the enumeration of mechanism structures. The remaining functional requirements are implemented in a "Tester" for the evaluation of the enumerated structures. The mechanisms that pass this initial screening are called potential mechanisms. At this stage, if a most promising mechanism can be identified, then that particular mechanism is chosen for detailed analysis and design optimization. Otherwise, all the potential mechanisms are analysed and the best mechanism is chosen for the design.

This method has a few advantages over the method proposed by Freudenstein and Maki. Since some of the functional requirements are implemented as structural characteristics in the generator, the search domain for candidate mechanisms is greatly reduced. This factor is especially useful in the development of an automated computer synthesis program.

1.2 Literature Review

A lot of previous work has been done on constant-velocity (CV) shaft couplings and differentials. Hunt (1973) gives a general theory for the construction of a CV coupling. The journal literature on gearless differentials is sparse even though a lot of work has been done on differential gears (Yan and Hsieh, 1994). Habil and Altmann (1950) explains coupler transmissions for uniform transmission ratios and especially concentrates on 1:-1 coupler transmissions.

In the aforementioned literature, there is no indication as to whether the authors have conducted a systematic exploration of all possible 1:-1 CV couplings and differentials. In this thesis, we develop a systematic search procedure to identify all the gearless 1:-1 CV couplings within a list of search specifications. These mechanisms are evaluated against a tester and potential mechanisms are obtained. Then, a most promising candidate mechanism is chosen and converted to a gearless differential mechanism and a detailed analysis is done on that mechanism.

1.3 Scope of the Thesis

In a vehicle, power generated by an engine goes through different mechanisms before it reaches the wheels. Typically, the power flows from the crank shaft of an engine to a transmission unit, followed by a a final reduction unit, then a gear differential, and then the wheels. The purpose of a differential is to transmit power from the final reduction unit to the two wheels of a vehicle and, at the same time, aids the vehicle in making a turn for which it is necessary that one wheel rotates faster than the other.

Conventional differentials use gears for power transmission. In this study, we point out the drawbacks with using gears and perform a feasibility study in the design of a differential without gears, called gearless differentials.

In this study, the systematic design methodology shown in Figure 1.1 is used to derive gearless differential mechanisms with a slight modification to the enumeration process. Instead of enumerating gearless differentials, 1:-1 CV shaft couplings are enumerated first. The reason for this choice is explained in the next Chapter. These enumerated mechanisms are then evaluated and potential 1:-1 CV couplings are obtained. A most promising mechanism is chosen and converted to a gearless differential mechanism. Then, detailed kinematic and dynamic analyses are performed to demonstrate the feasibility of the mechanism.

1.4 Organization of the Thesis

Chapter 2 explains the principles of operation behind a 1:-1 CV shaft coupling and a differential mechanism. It also illustrates the need for a gearless differential and the way to convert a 1:-1 CV coupling to a differential mechanism. Chapter 3 explains the enumeration procedure adopted in detail. The "Generator" and the "Tester" in Figure 1.1 are listed out for the enumeration of the 1:-1 CV couplings and all the possible mechanisms within the scope of the "Generator" are enumerated. Chapter 4 uses the "Tester" to evaluate all the enumerated mechanisms which results in a set of potential mechanisms. Also, one of the potential mechanism is chosen and converted to a differential mechanism.

Chapter 5 deals with detailed kinematic and dynamic analyses on both the chosen 1:-1 CV coupling and the gearless differential. Kinematic analysis is done

both analytically and using the software package DADS (CADSI, 1993), while the dynamic analysis is done entirely by the simulation model using DADS. Chapter 6 uses the results obtained from the kinematic and dynamic analyses to generate design guidelines for choosing appropriate link lengths. Finally, chapter 7 summarizes this work, briefly explains an alternate design, and suggests some future extentions.

Appendix A explains the derivations for the velocities of the centers of the two wheels when the vehicle is moving in a curved path and appendix B explains the masses and moment-of-inertia properties of the various links used in the DADS simulation model.

Chapter 2

Principles of Operation

2.1 Principle of 1:-1 Constant-Velocity Shaft Couplings

The objective of a 1:-1 CV shaft coupling is to obtain a constant 1:-1 angular velocity ratio between the input and the output shaft. An example mechanism is shown in Figure 2.1 which is usually used as a bevel-gear differential mechanism. For this mechanism to function as a 1:-1 CV shaft coupling, link 2 serves as the input link, link 4 serves as the output link, and the cage or carrier (link 1) is fixed to the ground. Since this is a one DOF(degree-of-freedom) mechanism, one independent variable (here the position of the input link) will completely determine the state of the system. The principle behind the mechanism in Figure 2.1 to function as a 1:-1 CV coupling is explained below.

Let

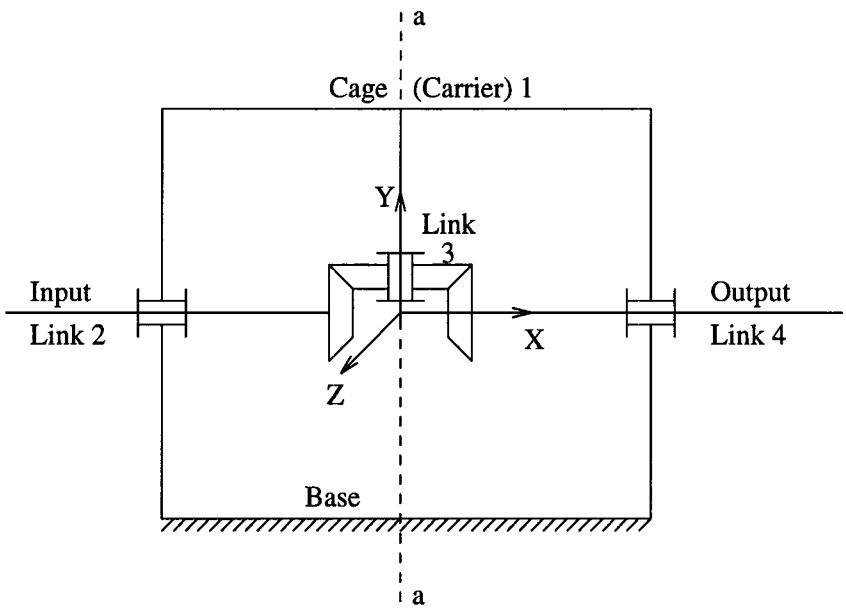

Figure 2.1: A 1:-1 CV shaft coupling

ω_2, ω_3, and ω_4	be the angular velocities of links 2, 3 and 4, respectively
N_2, N_3, and N_4	be the number of teeth on the gears mounted on links 2, 3 and 4, respectively

Let link 2 be rotating about the positive X-axis with an angular velocity of ω_2. This causes the gear mounted on link 3 to rotate with an angular velocity of ω_3 about the positive Y-axis with the following relation between the two:

$$\frac{\omega_2}{\omega_3} = \frac{N_3}{N_2} \tag{2.1}$$

The rotation of gear 3 causes the output link 4 to rotate at an angular velocity of ω_4 about the negative X-axis which satisfies the following equation:

$$\frac{\omega_3}{\omega_4} = -\frac{N_4}{N_3} \tag{2.2}$$

The negative sign in Eq. (2.2) indicates that the output shaft rotates in the negative X direction. At this stage, we introduce the constraint that the number of teeth on gear 2 is equal to the number of teeth on gear 4. That is

$$N_2 = N_4 \tag{2.3}$$

Hence, from Eqs. (2.1), (2.2) and (2.3), we get

$$\omega_2 = -\omega_4 \tag{2.4}$$

Eq. (2.4) proves that the angular velocities of the input shaft and the output shaft are equal in magnitude but opposite in direction of rotation. This can be clearly understood when we carefully examine the motion of the gears in Figure 2.1. If the input link 2 rotates about the positive X-axis, then the gear on link 3 will rotate about the positive Y-axis, while the output link 4 will rotate about the negative X-axis according to the right-hand-rule. So a constant 1:-1 angular velocity ratio between the input and ouput shafts is obtained thus achieving a 1:-1 CV coupling.

One important application of a 1:-1 CV shaft coupling is that, with a little modification, it can be transformed into a differential mechanism. This conversion is explained in following sections.

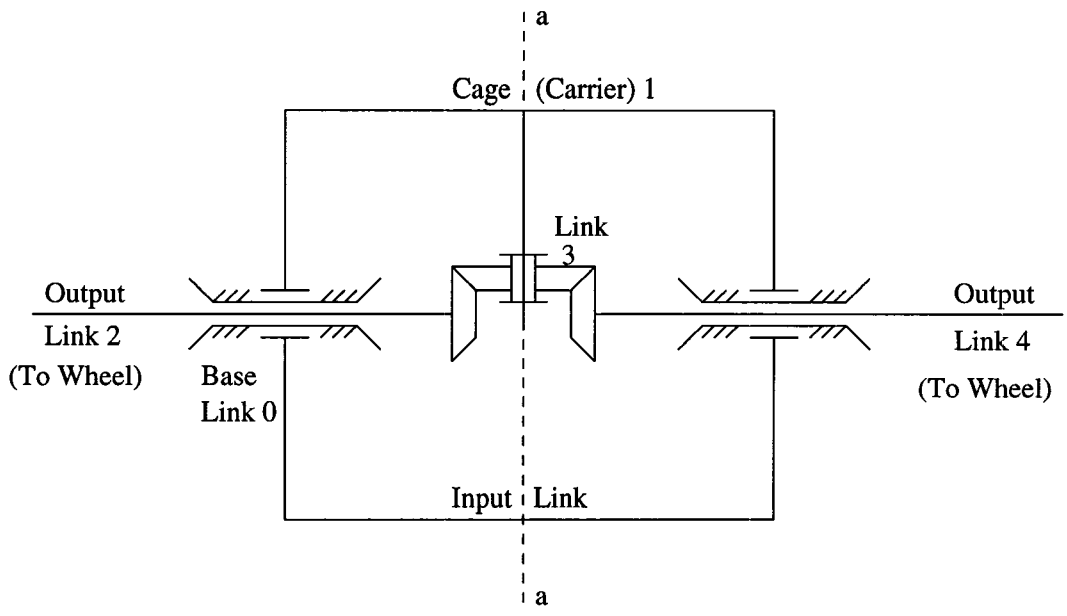

Figure 2.2: Corresponding differential mechanism

2.2 Principle of Differential Mechanisms

The basic principle of operation of a differential mechanism is the same as a 1:-1 CV shaft coupling but it serves a totally different purpose in automobiles. Differential mechanisms are often used as a transmission device, which transmits power from an engine to the wheels of an automobile. Figure 2.2 shows a typical bevel-gear differential mechanism.

In this mechanism, the cage or carrier (link 1) serves as the input link while the two shafts (links 2 and 4) serve as the output links of the differential mechanism. This mechanism is a two-DOF mechanism which implies that we need two independent variables to determine the state of the system. One is the rotation of the cage (which is the input to the mechanism) and the other is a constraint imposed by the no-slip condition. This no-slip condition means that both the wheels must not slip at their respective points of contact with the ground. This

yields a definite speed ratio between the two wheels as a function of the radius of a turn. This fact is observed quite clearly when a car gets stuck in snow, one wheel would be rotating freely while the other would be stationary thus stalling the car. When there is no friction (or very little) between the freely rotating wheel and the ground, the friction constraint is not properly imposed and the differential mechanism is not able to perform its function.

The functioning of a differential mechanism can be assumed as a superposition of two different motions. One motion is that, with the cage locked, the mechanism functions as a 1:-1 CV coupling. This motion attributes to the differential speed of the wheels, say ω_{diff}. That is, if one wheel rotates at a differential speed of ω_{diff} rad/s, then the other wheel will rotate at $-\omega_{diff}$ rad/s, thus functioning as a 1:-1 CV coupling. The other motion is that the whole differential mechanism rotates as a rigid body about the axis of the wheels. In this case, both output shafts would rotate along with the cage at the same speed. These two motions, when superposed on one another results in the motion of a differential mechanism. This is explained in greater detail in Chapter 5.

Differential mechanisms are used in automobiles to produce the differential motion that is necessary for making a turn. When an automobile is making a turn, one wheel will rotate faster than the other thus aiding the turn. This difference in speed of the output shafts is attributed to the principle of differential mechanisms.

2.3 Need for Gearless Differentials

Conventional differential mechanisms are made by using gears. One main disadvantage of using gears is that each gear-pair has a line contact, which results in severe wear and tear of the gears. The useful life of such a mechanism is compromised due to this fact. Another disadvantage is the higher cost of manufacturing and potential noisiness associated with the gear-pairs.

On the other hand, let us consider a revolute joint connecting two links. The nature of contact between the two links of a revolute joint is a surface contact. The stress and wear to the links is reduced due to this fact. So links connected together by joints with surface contact gain the advantage of longer life span. Thus there is a need to replace the differential gears with differential linkages. In the following chapters, gearless CV couplings and differentials are enumerated and analyzed, to overcome the above mentioned problems.

2.4 A 1:-1 CV Coupling and Its Corresponding Differential Mechanism

As mentioned earlier, the method adopted in this work is to initially enumerate all the 1:-1 CV shaft couplings and to evaluate them. Then, a promising mechanism is chosen and converted to a gearless differential mechanism for further analysis. The conversion is done as follows.

We note that an inversion and an addition of one coaxial link to the mechanism shown in Figure 2.1 results in a two-DOF differential mechanism shown in Figure 2.2. This is a straightforward conversion that is employed in this study.

The addition of a coaxial link converts a one-dof CV coupling to a two-dof differential mechanism. The inversion comes from the fact that in a 1:-1 CV coupling, link 2 is the input shaft and the carrier is fixed to the ground, while in a differential mechanism, the carrier serves as the input link and the two coaxial shafts, links 2 and 4, form the output links.

Chapter 3

Enumeration of 1:-1 CV Couplings

As mentioned previously, the first step is to systematically enumerate 1:-1 CV shaft couplings. This chapter deals with the enumeration process in detail and also explains some problems that can occur in the mechanisms especially the situation for which singular conditions may occur. The method adopted for the systematic enumeration is as shown in Figure 1.1. First, the functional requirements are identified. Then, some of the requirements are translated into the structural characteristics of 1:-1 CV couplings. Finally, a class of 1:-1 CV couplings are enumerated and evaluated according to the structural characteristics and other functional requirements.

3.1 Functional Requirements

The most important functional requirement of a CV shaft coupling is the ability to provide a constant angular velocity ratio between the input and output shafts, in this case the ratio being 1:-1. Another important functional requirement that is of particular interest in this work is the ability to transform such a 1:-1 CV coupling to a differential mechanism.

3.2 Structural Characteristics

One of the most important problems that arises in a 1:-1 CV shaft coupling is the existence of singularity conditions. Habil and Altmann (1950) emphasized mainly on the occurence of singular points and different ways of avoiding it. A simple example explained below illustrates the occurence of singular points in 1:-1 CV shaft couplings.

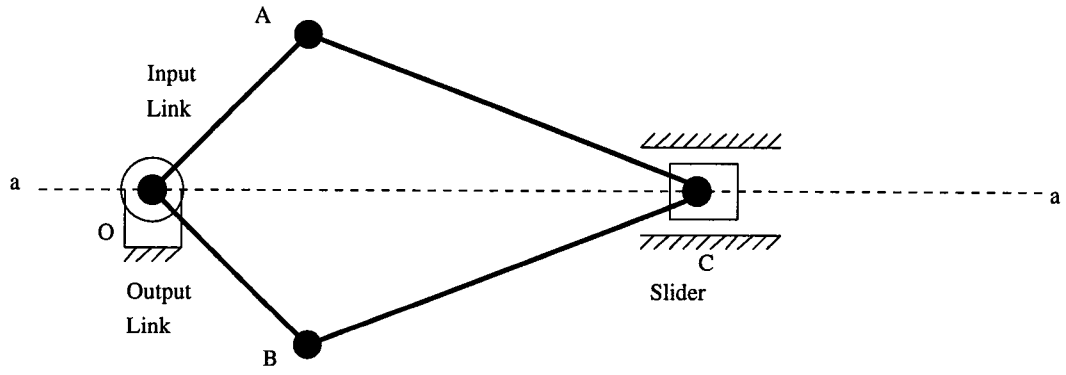

Figure 3.1: Existence of singularity conditions

For the planar six-link mechanism shown in Figure 3.1, links OA = OB and AC = BC. When the input link OA rotates in one direction about pivot O, the output link OB will rotate in the opposite direction with the same angular speed, thus acting as a 1:-1 CV coupling. But at the instant of time when the slider C is at one of its extreme positions, i.e. both OA and OB are aligned with the axis a-a, link OB has the possibility of rotating in either directions, either along with link OA thus becoming a 1:1 CV shaft coupling or in the opposite direction of link OA thus remaining as a 1:-1 CV shaft coupling. This condition is called the singular condition and the two extreme points are called the singular points. Singularity free condition is a very important functional requirement as it may eliminate a whole class of mechanisms which possess singular points. Habil and

Altmann (1950) came up with a few spatial mechanisms which overcome this kind of singular conditions. Recently, Ricardo Consulting Engineers Ltd. (see Moore and Greenwood, 1994) developed a spatial gearless differential mechanism from one of them.

In this study, the search is restricted to one-dof spatial mechanisms since planar mechanisms either result in having singular points or too many prismatic pairs (see Habil and Altmann, 1950) both of which are undesirable. Also work has been done previously on planar mechanisms (though not systematically) but not in spatial 1:-1 CV shaft couplings.

The joints to be considered in this work are turning pairs (R), prismatic pairs (P), cylindrical pairs (C), spherical pairs (S) and ball-in-cylinder (Bc) pairs. Only lower pairs are considered due to the high load-carrying capability of these joints. The Bc-pair is also included because of its ease of manufacture even though it is not a lower pair. Also since its freedom is equal to four, it helps in reducing the number of links and thus reducing the complexity and inertia of a mechanism. The plane pair (E) is not considered even though it is a lower pair as it can slide in two dimensions which may result in excessive friction.

Hunt (1973) describes the necessity of symmetry of a mechanism about the plane bisecting the input and the output shaft axes for it to act as a CV shaft coupling. This holds true for a single loop mechanism with a desired velocity ratio of 1:1. It turns out that this same necessary condition also holds for 1:-1 CV couplings with two independent loops. It can be seen from Figure 2.1 that the bevel-gear 1:-1 CV coupling is symmetric about the axis a-a and it has two loops. A detailed explanation as to why this works is given below.

Mechanisms with two independent loops are considered as they replicate a

standard differential gear mechanism as shown in Figure 2.2, the only difference being the gear pairs are replaced by the kinematic-pairs chosen above. The main reason behind this decision is that these two-loop couplings can be easily transformed to a differential mechanism which is the main aim of this work. Figure 2.2 shows the presence of a middle-joint (an R-pair in this case) and a middle ternary link which transmits motion to the two shafts when the cage is given an input. Figure 2.2 also shows that the two output links of the differential mechanism are coaxial and that they are both supported by the same carrier. All these facts are incorporated into the structural characteristics of 1:-1 couplings.

A general mechanism schematic satisfying the condition of symmetry and the condition of two coaxial output links with a joint in the middle and two coaxial R-joints is shown in Figure 3.2. The "mechanisms" shown in the rectangular boxes are to be synthesized. Because of the symmetry, the mechanism can be split into two halfs as shown in Figure 3.3. We note that the two halves share two ternary links and one common joint. One of the ternary links, link 1, serves as the carrier while the other, link 4, serves as a lever to transmit motion from one half of the mechanism to the other half. In addition, each half of the mechanism is a one-dof kinematic chain.

Consider the left half of the mechanism as shown in Figure 3.3(a). As the input link 2 rotates, the lever 4 will produce some motion. Now consider the motion of the lever 4 as the input to the right half of the mechanism as shown in Figure 3.3(b). Since the right half of the mechanism is a mirror image of the left half about the plane of symmetry, the output link 6 of the right half will rotate in the opposite direction at the same rate as the input link 2 of the left half. Hence the entire mechanism works as a 1:-1 CV shaft coupling.

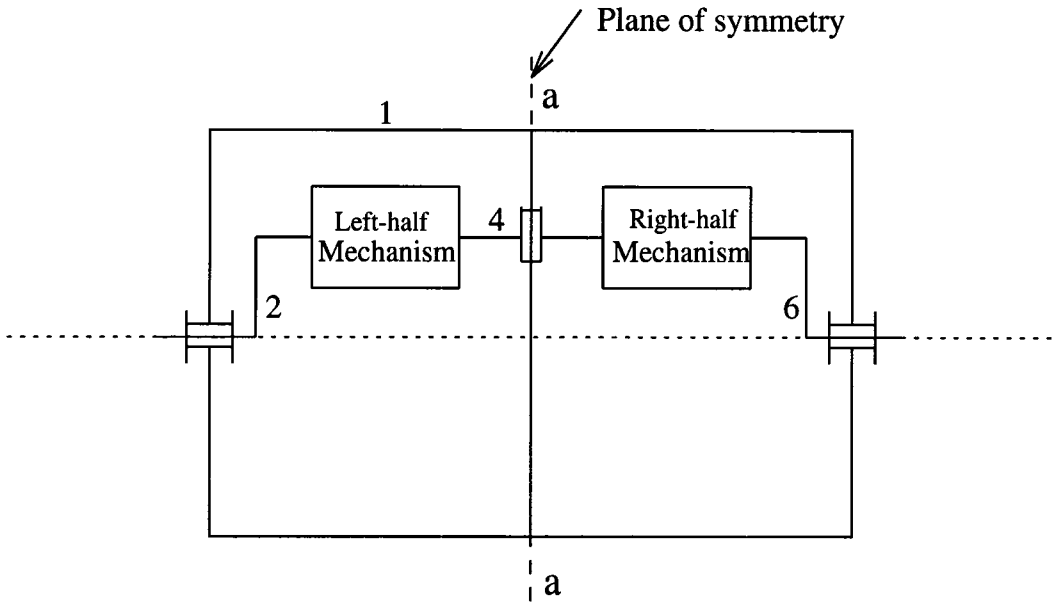

Figure 3.2: A general 1:-1 CV coupling

Next, a decision on the type of middle joint is made. Both R-pair and P-pair cannot be the middle joint since the resulting mechanisms will possess singular conditions. The reason is that if an R-pair is used as the middle joint, each half will function as a spatial crank-and-rocker mechanism which has two extreme singular positions. Similar reason holds for a mechanism with a P-pair in the middle. If the middle joint is an S-pair, then the middle link is capable of rotating about any axis passing through the center of the S-pair. The symmetry of such a mechanism will be lost when the middle link rotates about an axis that is not parallel to the plane of symmetry. Losing the symmetry implies that the mechanism will no longer function as a 1:-1 CV shaft coupling. So S-pair as the middle joint is also rejected. Similar problem is faced with Bc-pair as the middle joint. With C-pair as the middle joint, the above problems are overcome since the C-pair is able to slide and rotate at the same time. This makes it possible

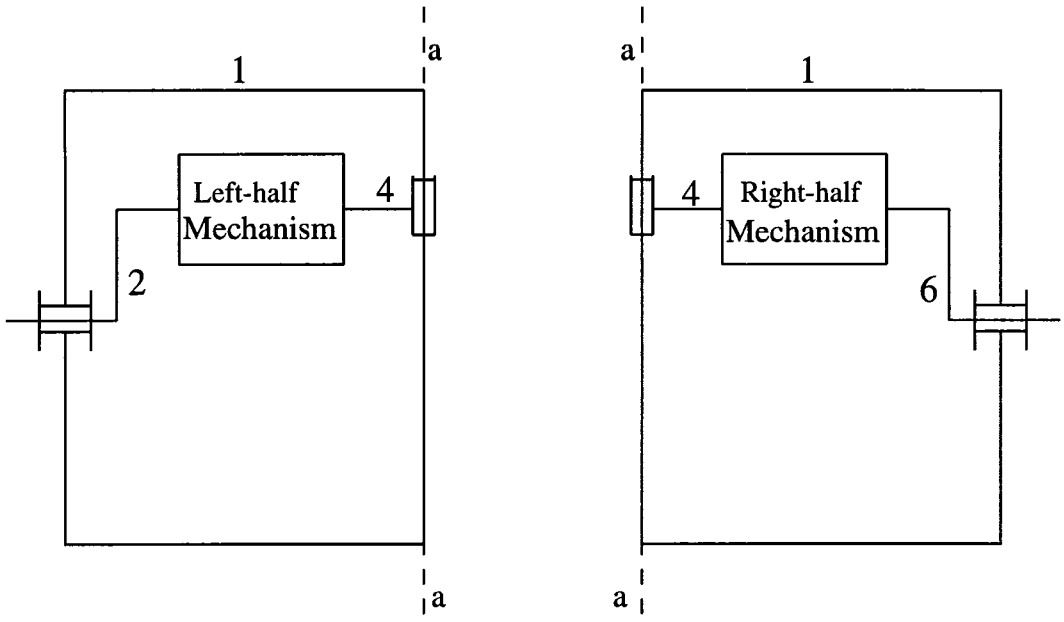

Figure 3.3: (a) The left half, (b) The right half

for the two ends of the lever to describe a full circle on a cylinder per rotation of the input link. Since the lever can perform a continuous motion, there will be no singular points. Hence the only feasible middle joint is a C-pair. All the above characteristics are summarized below as search specifications (Generator) and evaluation criteria (Tester).

3.2.1 Structure Specifications

- The search is limited to spatial mechanisms.
- The joints to be considered are turning pairs (R), prismatic pairs (P), spherical pairs (S), cylindrical pairs (C), and ball-in-cylinder pairs (Bc).
- The search is restricted to only those mechanisms with two independent loops.

- The cage (base-link) is a ternary link (i.e., it has three joints). This link is actually the input link of a differential mechanism. The middle joint connects the cage to the middle link which is the second ternary link. All the other links are binary.

- The input and output links must be coaxial and they must both be supported by the cage.

- The joints connecting the input and output links with the cage are R-pairs. This means that the cage has two inline R-pairs (the third joint is the middle joint).

- The middle joint is a C-pair with its joint axis perpendicular to the joint axis of the input and output links.

- The maximum number of joints in a mechanism is limited to seven. This controls the size of a mechanism from becoming too big thus making the mechanism more portable.

- To achieve a 1:-1 ratio from the input to the output link, the symmetry of a mechanism about the plane bisecting the shaft axes must be maintained. This plane of symmetry splits the mechanism into two sub-mechanisms, each of them has one degree-of-freedom (satisfying the general degree-of-freedom equation).

- There is one common joint (the middle joint) and two common links (the middle link and the cage) between these two sub-mechanisms.

3.2.2 Evaluation Criteria

- The maximum number of prismatic and cylindrical pairs cannot exceed three. (This limits the amount of sliding in a mechanism, thus reducing frictional energy loss, wear and tear).

- No link can have more than one sliding pair. (This again limits the amount of sliding in a mechanism).

3.3 Enumeration of 1:-1 CV Shaft Couplings

Based on the structural characteristics listed above, two partially labelled graphs representing all possible 1:-1 CV shaft couplings with upto six links are shown in Figures 3.4 and 3.5, where X and Y denote the unknown joints that are to be enumerated. The correspondence between the graphs and their structural diagrams is that the links are represented by vertices, joints by edges, and the joint connection of links correspond to the edges connection of vertices. The edges are labelled according to the joint type and the fixed link is identified with a circle around the vertex.

Each graph contains two loops and each loop represent a one-dof mechanism which satisfies the general degree-of-freedom equation:

$$F = \lambda(l - j - 1) + \sum_{i=1}^{j} f_i \tag{3.1}$$

where

F : degrees of freedom of a mechanism, $F = 1$

λ : mobility number, $\lambda = 6$ for spatial mechanisms

l : number of links

j : number of joints

f_i : degrees of freedom permitted by the i^{th} joint

For each loop,

$$j = l \tag{3.2}$$

Substituting Eq. (3.2), $F = 1$, and $\lambda = 6$ into Eq. (3.1) yields

$$\sum_{i=1}^{j} f_i = 7 \tag{3.3}$$

That is the sum of degress of freedom associated with all the joints in each loop must be equal to seven.

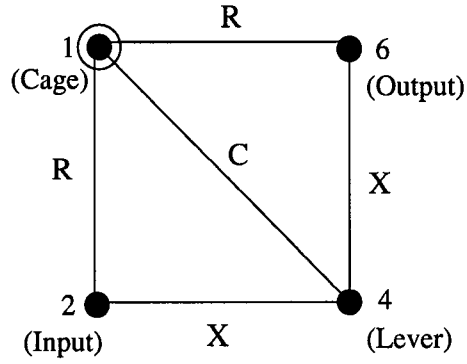

Figure 3.4: Four-link mechanism

Applying Eq. (3.3) to one of the loops of the mechanism shown in Figure 3.4, we obtain $f_x + 1 + 2 = 7$, where f_x denotes the degrees of freedom permitted by the X joint. Hence $f_x = 4$ and X can only be a Bc pair. Only one joint combination is possible and it is RBcCBcR.

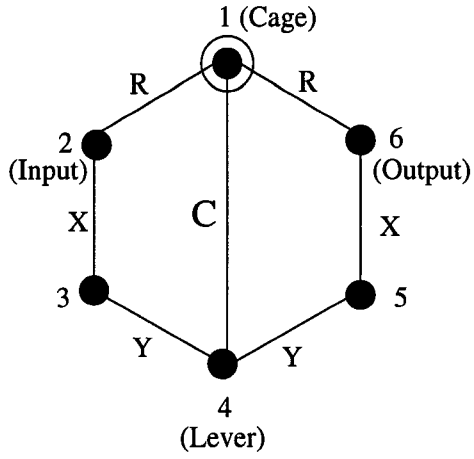

Figure 3.5: Six-link mechanism

For the mechanism shown in Figure 3.5, we have $f_x + f_y + 1 + 2 = 7$, where f_x and f_y denotes the degrees of freedom permitted by the X and Y joints respectively. Hence, $f_x = f_y = 2$, or $f_x = 3$ and $f_y = 1$, or $f_x = 1$ and $f_y = 3$. With these values of f_x and f_y, five joint combinations are possible. They are RCCCCCR, RRSCSRR, RSRCRSR, RPSCSPR and RSPCPSR.

These are the only possible mechanisms that can be obtained using the search specifications. All the different joint combinations obtained are summarized in Table 3.1. The graphs and their corresponding couplings are sketched in Figure 3.6. The following notation applies for all diagrams:

1	:	fixed link (cage or carrier)
2	:	input link
3 and 5	:	coupler links
4	:	lever (middle link)
6	:	output link

Table 3.1: Table of enumerations

	Different Joint Combinations
1.	RBcCBcR
2.	RCCCCCR
3.	RRSCSRR
4.	RSRCRSR
5.	RPSCSPR
6.	RSPCPSR

Each of the structures is a one degree-of-freedom mechanism consisting of two loops connected together by the middle C-pair and the symmetry about the plane bisecting the shaft axis is responsible for the 1:-1 velocity ratio between the input and output shafts.

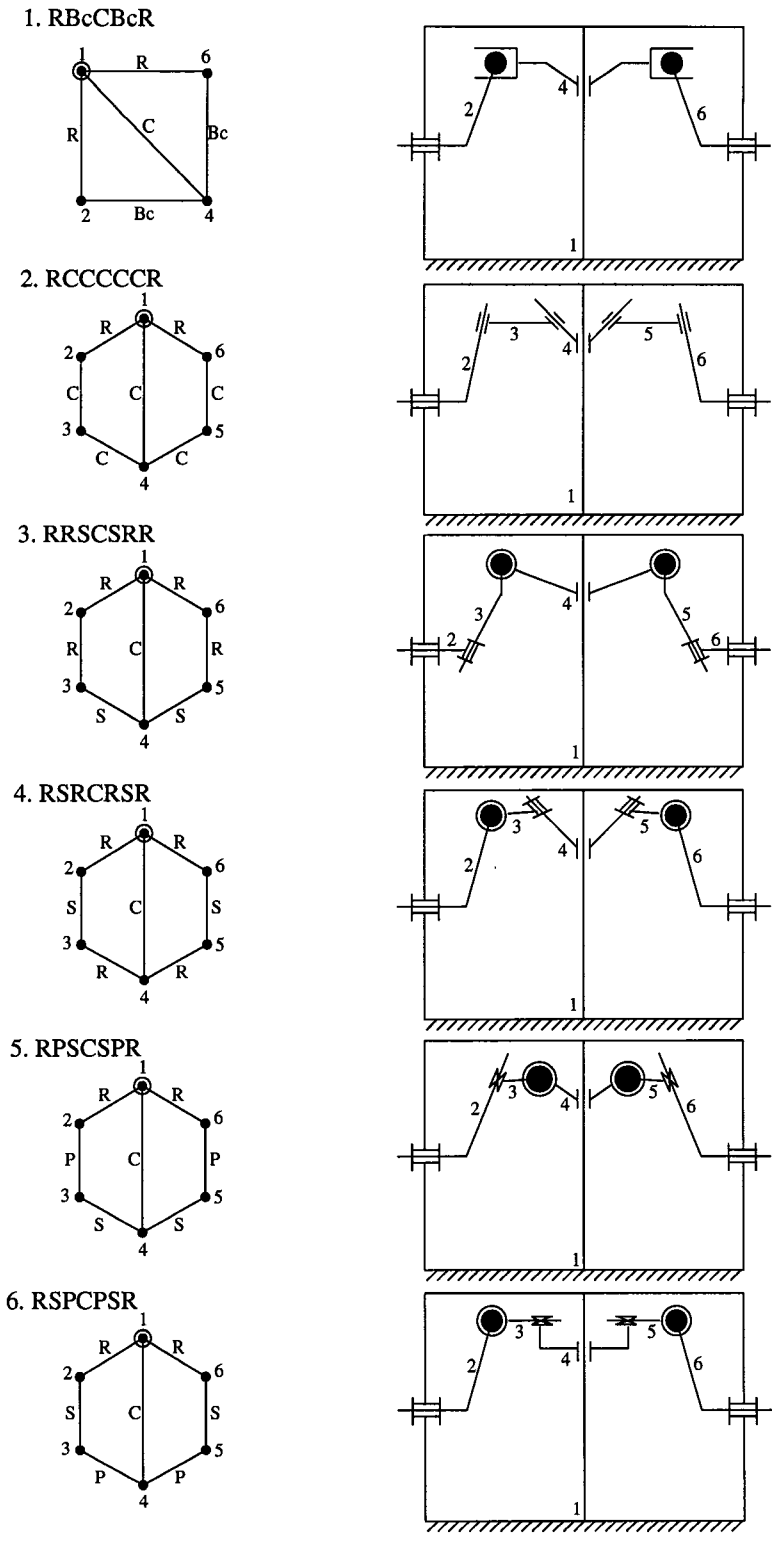

Figure 3.6: Enumerated graphs and corresponding mechanisms

Chapter 4

Structural Evaluation

Applying the systematic design of methodology depicted in Figure 1.1 resulted in six 1:-1 CV shaft couplings as shown in Figure 3.6. That was the "generator" stage where all possible mechanisms are enumerated based on some of the structure specifications. In this chapter, the mechanisms are filtered through a "tester" to obtain a set of potential mechanisms. The criteria for the tester have already been summarized as the evaluation criteria in the previous chapter. The evaluation process is explained below.

4.1 Potential Mechanisms

Each of the mechanisms in Figure 3.6 is evaluated against the tester and the results are summarized in Table 4.1. Any mechanism that passes the test is termed as a potential mechanism. The application of the evaluation guidelines resulted in four potential mechanisms.

An interesting feature is noted about the mechanisms enumerated. The degrees of freedom for the whole mechanism, calculated by using the general degree-of-freedom equation, Eq. (3.1), is zero as shown below.

Table 4.1: Evaluation of Mechanisms

Mechanism	Evaluation
RBcCBcR	Acceptable as a potential mechanism. Even though this mechanism has two Bc pairs (which are not lower pairs), the small number of links in the mechanism is an advantage.
RCCCCCR	Reject : The presence of too many cylindrical pairs in the mechanism can cause excessive sliding friction.
RRSCSRR	Acceptable as a potential mechanism.
RSRCRSR	Acceptable as a potential mechanism.
RPSCSPR	Acceptable as a potential mechanism.
RSPCPSR	Reject : The lever has three sliders which can cause excessive sliding on the lever link.

For mechanism number 1, we have $\lambda = 6$, $l = 4$, $j = 5$, and $\sum f_i = 1 + 4 + 2 + 4 + 1 = 12$. Hence, we have

$$F = 6(4 - 5 - 1) + 12 = 0 \tag{4.1}$$

Similarly, for the other mechanisms, we have $\lambda = 6$, $l = 6$, $j = 7$, and $\sum f_i = 12$. Again, we have

$$F = 6(6 - 7 - 1) + 12 = 0 \tag{4.2}$$

Even though these mechanisms are one degree-of-freedom mechanisms, they do not obey the general degree-of-freedom equation. Those mechanisms which do not satisfy the general degree-of-freedom equation are called overconstrained mechanisms (see Mavroidis and Roth, 1995a and 1995b). Thus all the mechanisms enumerated are overconstrained mechanisms.

Next, we choose a most promising coupling from among the four potential mechanisms. An examination of the potential mechanisms shows that the RBc-CBcR mechanism is the mechanism suggested by Habil and Altmann (1950) as a 1:-1 CV coupling and developed by the Ricardo Consulting Engineers Ltd as a differential mechanism. Even though this mechanism has fewer number of links than the others, it is not judged as the most promising mechanism. This is because the mechanism has two Bc pairs, which may result in high stress due to the point contact in the joints.

The RPSCSPR mechanism contains three sliders while the RRSCSRR mechanism and the RSRCRSR mechanism have only one slider each. Since more number of sliders implies more friction, we eliminate the RPSCSPR mechanism as the most promising mechanism. The number of sliders is an important criterion especially when the mechanism is used as a high-speed 1:-1 CV coupling.

Hence, we are left with two mechanisms: RRSCSRR and RSRCRSR mechanisms. Both these mechanisms are quite similar, the only difference being the relative arrangement of the R-pair and S-pair.

4.2 The Most Promising 1:-1 CV Coupling

Since there is not much difference between the RRSCSRR and RSRCRSR mechanisms, either one of them could serve as the most promising mechanism. In what follows, we choose the RRSCSRR mechanism as the most promising mechanism and perform detailed kinematic and dynamic analysis on this mechanism. A schematic diagram of the coupling is shown in Figure 4.1.

The mechanism consists of six links and seven joints and all the joints are lower pairs. The lever and the cage are ternary links while all the other links are binary links. The input link 2 is connected to a coupler link 3 by an R-pair, which in turn is connected to the lever 4 by an S-pair. The C-pair in the middle connects the lever with the cage and the symmetry of the mechanism is maintained about the axis of this C-pair. As explained before, this symmetry in the mechanism is responsible for the mechanism to function as a 1:-1 constant-velocity shaft coupling. The lever transfers motion from one half of the mechanism to the other half by oscillating as well as sliding along its cylindrical axis simultaneously. We can visualize the two ends of the lever (where the S-pairs are located) as performing a motion along a circular path on a cylinder whose axis coincide with the axis of the C-pair. The singular condition is avoided due to this continuous motion of the lever.

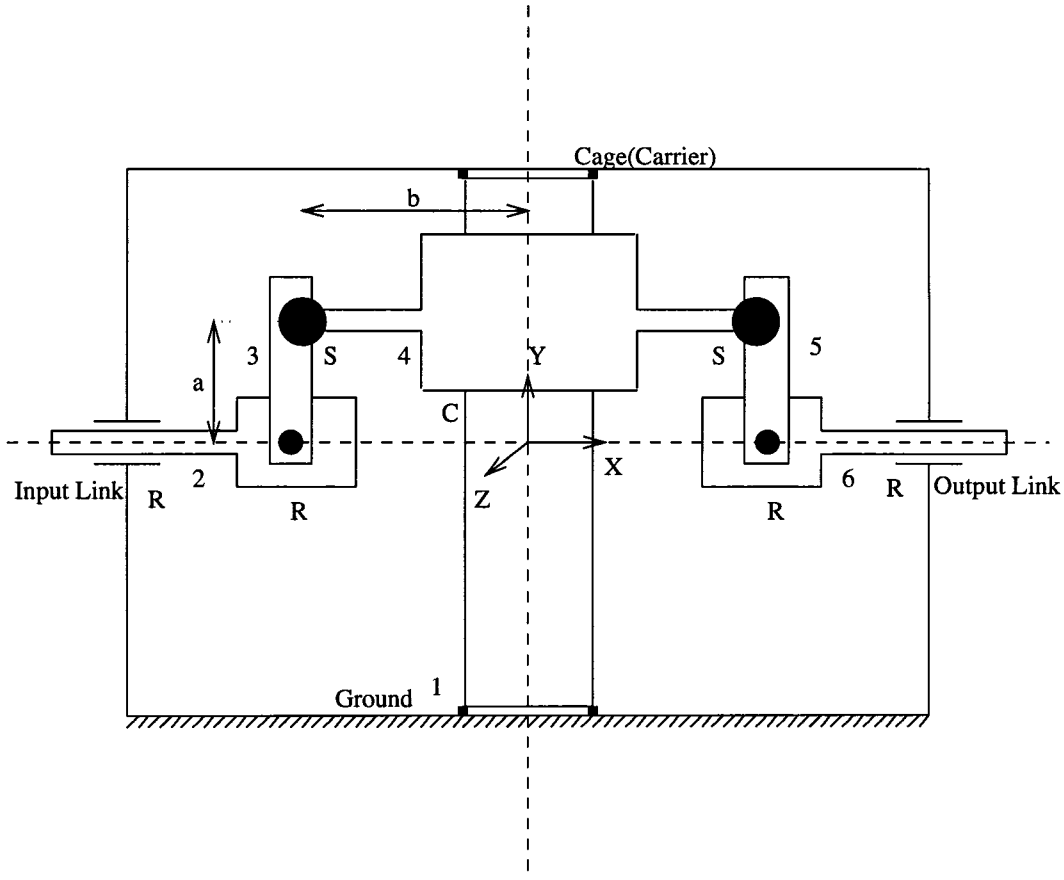

Figure 4.1: The most promising 1:-1 CV coupling

4.3 Conversion to a Gearless Differential Mechanism

The 1:-1 CV shaft coupling obtained above is now transformed into a differential mechanism. As explained before, an inversion and an addition of one more link to the coupling results in a differential mechanism. A sketch of the gearless differential is shown in Figure 4.2.

The inversion comes from the fact that the cage in the coupling becomes the input link in the differential, while the newly added link becomes the fixed link

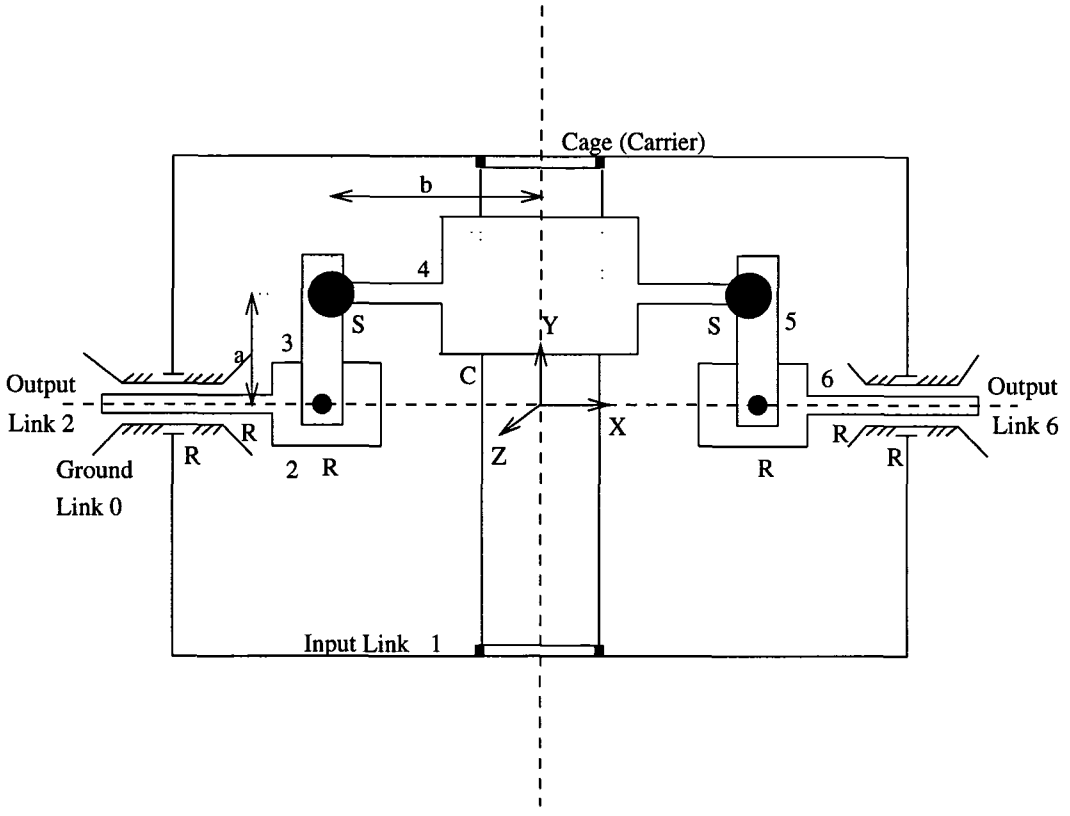

Figure 4.2: The most promising gearless differential

for the differential. As this mechanism is a two degree-of-freedom mechanism, it has the two coaxial links as the output links whereas in the coupling, one of the coaxial link serves as the input link and the other as the output link.

Chapter 5

Kinematic and Dynamic Analyses

In the previous chapter, a promising mechanism has been chosen. In this chapter, a detailed kinematic and dynamic analysis will be performed to ensure that the mechanism does have the potential for use as a gearless differential. Kinematic analysis is performed both by an analytical method as well as using the software package DADS, while the dynamic analysis is done fully on a simulated model by using DADS. The subsequent sections explains the analysis in detail.

5.1 Kinematic Analysis

5.1.1 Analytical Method

When the mechanism functions as a 1:-1 CV shaft coupling, the velocity ratio between the input and output shafts is 1:-1. That is, the output shaft rotates at the same speed as the input shaft but in the opposite direction. But when the same mechanism functions as a differential, the cage serves as the input and the two coaxial shafts function as the two output links to drive the wheels of a vehicle. In what follows, we derive an expression for the velocities of these

output shafts for a given input angular velocity of the cage.

Let

ω_{cage}	:	angular velocity of the cage with respect to the chassis of the vehicle
ω_2, ω_6	:	angular velocities of the two output shafts (wheels) with respect to the chassis of the vehicle
ω_{diff}	:	differential speed
x	:	distance between the two wheels of a vehicle
R_{curve}	:	radius of curvature of the path
r	:	radius of the wheels of a vehicle

We note that there are two different angular rotations involved in the motion of the vehicle which the reader must be aware of. One is the rotation of the whole vehicle about the center of curvature with respect to the ground since the vehicle is moving in a curve. The other is the rotation of the two wheels as well as the cage of the differential which is with respect to the chassis of the vehicle. These two rotations must be distinguished clearly.

The differential speed refers to the angular velocity of one of the wheels when the cage is locked. However, when the cage is locked, the mechanism functions as a 1:-1 CV shaft coupling. Thus the other wheel will rotate at the same speed but in the opposite direction. Hence, if one wheel rotates at a differential speed of ω_{diff} rad/s, then the other wheel will rotate at $-\omega_{diff}$ rad/s.

Another case to be considered is when the whole differential mechanism functions as one rigid body. Thus, both the output shafts would rotate along with the cage at a speed of ω_{cage} rad/s. In this case there is no differential at all.

Now, by applying the principle of superposition to the above two cases, we can obtain the angular velocities of the two shafts as

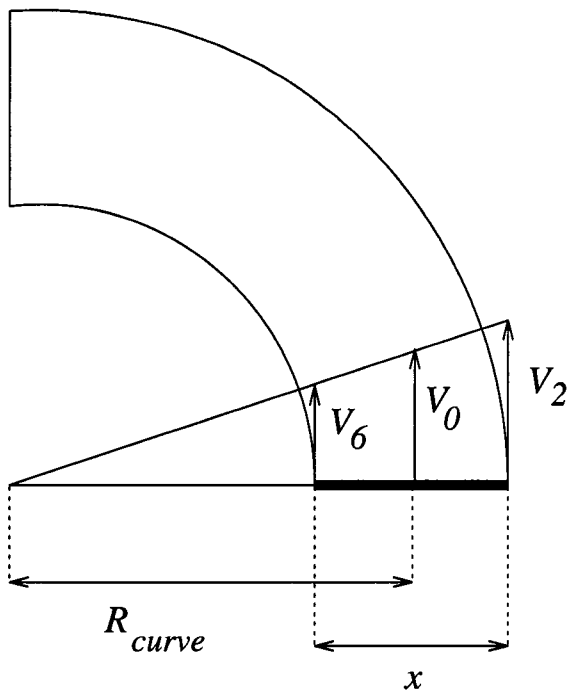

Figure 5.1: A vehicle moving in a curve

$$\omega_2 = \omega_{cage} + \omega_{diff} \tag{5.1}$$

and

$$\omega_6 = \omega_{cage} - \omega_{diff} \tag{5.2}$$

Consider the situation when the vehicle is making a turn which has a radius of curvature R_{curve} as shown in Figure 5.1. Let the linear velocity at the center of the vehicle be V_0 and the linear velocities of the center of the two wheels be V_2 and V_6 respectively, assuming $V_2 > V_6$. Referring to Appendix A, we obtain the following equations of constraint relating these velocities, the radius of curvature and the distance between the two wheels,

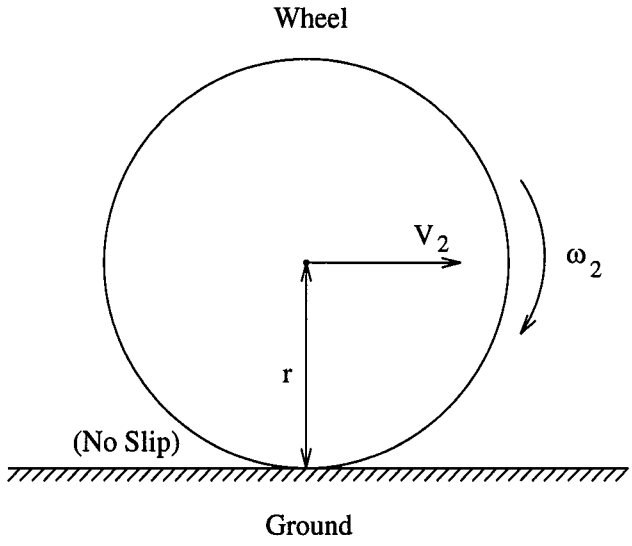

Figure 5.2: The rotation of a wheel

$$V_2 = V_0 \frac{(R_{curve} + x/2)}{R_{curve}} \tag{5.3}$$

and

$$V_6 = V_0 \frac{(R_{curve} - x/2)}{R_{curve}} \tag{5.4}$$

Now, consider the rotation of a wheel as in Figure 5.2. Here, we assume that wheel does not slip (or skid) which implies that the velocity of the point of contact on the wheel with the ground is zero. This assumption gives us the velocity of the center of the wheel as

$$V_2 = \omega_2 r \tag{5.5}$$

Similarly for the other wheel, we obtain,

$$V_6 = \omega_6 r \tag{5.6}$$

Therefore, from Eqs. (5.5) and (5.6), we get

$$\omega_2/\omega_6 = V_2/V_6 \tag{5.7}$$

Dividing Eq. (5.1) by Eq. (5.2), we obtain

$$\omega_2/\omega_6 = \frac{\omega_{cage} + \omega_{diff}}{\omega_{cage} - \omega_{diff}} \tag{5.8}$$

Dividing Eq. (5.3) by Eq. (5.4), we obtain

$$V_2/V_6 = \frac{(R_{curve} + x/2)}{(R_{curve} - x/2)} \tag{5.9}$$

Hence, substituting Eqs. (5.8) and (5.9) into Eq. (5.7), we get

$$\frac{\omega_{cage} + \omega_{diff}}{\omega_{cage} - \omega_{diff}} = \frac{(R_{curve} + x/2)}{(R_{curve} - x/2)} \tag{5.10}$$

By applying the rule of componendo and dividendo to Eq. (5.10), we get

$$\omega_{cage}/\omega_{diff} = \frac{R_{curve}}{x/2} = 2R_{curve}/x \tag{5.11}$$

or

$$\omega_{diff} = \frac{x}{2R_{curve}}\omega_{cage} \tag{5.12}$$

Substituting ω_{diff} into Eqs. (5.1) and (5.2), we obtain the angular velocities of the two wheels as

$$\omega_2 = \omega_{cage}(1 + \frac{x}{2R_{curve}}) \tag{5.13}$$

and

$$\omega_6 = \omega_{cage}(1 - \frac{x}{2R_{curve}}) \tag{5.14}$$

Thus, we have obtained expressions for the velocities of the two wheels as functions of the input cage velocity and the radius of the turn. In what follows, we evaluate the above equations for an interesting case. When the vehicle moves in a straight line, which implies that R_{curve} tends to infinity, then from equation (5.12), we obtain a zero differential speed. We also have $\omega_2 = \omega_6 = \omega_{cage}$. This implies that there is no internal motion within the differential and that the whole mechanism rotates as one rigid body. Hence, as long as the vehicle moves in a straight line, the differential acts as a rigid body to transmit motion from the carrier to the wheels.

From the above discussion, it is quite clear that the differential mechanism works as a superposition of a 1:-1 CV shaft coupling and a rigid body rotation. When the whole mechanism functions as one rigid body, there is no relative motion between the links. First, the kinematics of the CV coupling is performed. Then it is superimposed on the motion of the cage to obtain the kinematics of the overall differential mechanism. The analysis is done as follows.

Perhaps, the most critical link is the lever which transfers the motion from one half of the mechanism to the other. Its motion determines the functioning of the whole mechanism. As explained earlier, the lever can simultaneously oscillate about as well as slide along its axis. Its position along the axis and its orientation about the axis determines the status of the link. The aim of this analysis is to determine the position and orientation of the lever for a given input angle of link 2. It is also clear that once we obtain the coordinates of the lever, the position of the coupler links 3 and 5 and the output link 6 can be found.

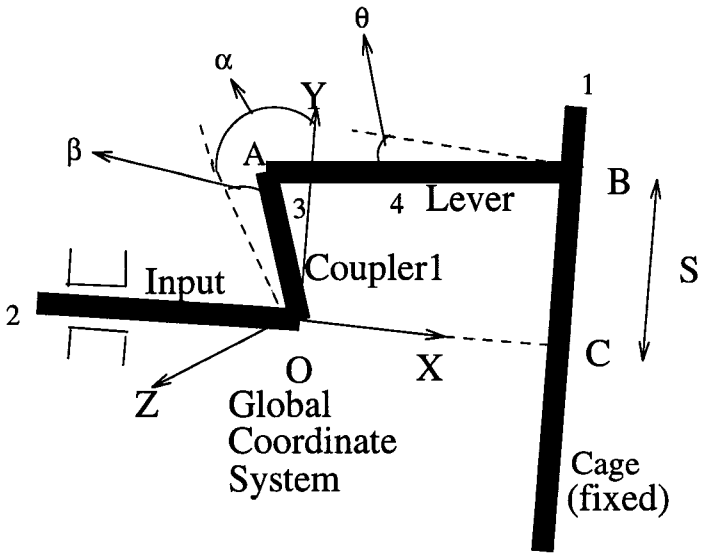

Figure 5.3: Kinematic Analysis

Consider just the left half of the mechanism as shown in Figure 5.3. For the purpose of analysis, an X-Y-Z coordinate system is defined with its origin located at the point of of intersection where the first and the second revolute joint axes intersect, its X-axis pointed along the axis of rotation of the input shaft and the Y-axis parallel to the cylindrical axis. The input shaft is given an input angle α with the cage fixed. As shown in Figure 5.3, let

α be the orientation angle of the input shaft measured from the global Y-axis,

β be the angle between the line OA and the projection of OA on to the global YZ plane,

θ be the orientation angle of the lever about the cylindrical axis. Specifically it is the angle between the line AB and a line parallel to the global X axis,

S be the displacement of the lever along the cylindrical axis (the distance between points B and C),

a be the length of the coupler link, $a = |OA|$,

b be the half length of the lever, $b = |AB|$.

The initial conditions are as follows:

$\alpha_{init} = 0$,

$\beta_{init} = 0$,

$\theta_{init} = 0$, and

$S_{init} = a$

The coordinates of point B with respect to the global coordinate system is (b, S, 0). To find the coordinates of point A, we project line AB along the X and Z axes and combine it with the coordinates of B. The projections of AB along the X and Z axes are $b\cos\theta$ and $b\sin\theta$, respectively. Hence, the coordinates of point A are

$$X_A = b - b\cos\theta = b(1 - \cos\theta) \tag{5.15}$$

$$Y_A = S \tag{5.16}$$

$$Z_A = b\sin\theta \tag{5.17}$$

Now we obtain the coordinates of point A in terms of the vector OA. The coordinates of point O is (0, 0, 0). Since the motion of the coupler is a complicated three dimensional motion, obtaining the coordinates of point A is not trivial. The motion of the coupler can be assumed to be a superposition of two different rotations: a rotation about the first revolute joint axis, connecting the input link to the ground, by an angle α followed by another rotation about the displaced second revolute joint axis, connecting the input link to the coupler, by an angle β as shown in Figure 5.4. It can also be considered as a rotation about the second revolute joint axis by an angle β followed by another rotation about the first revolute joint axis by an angle α. The resulting coordinates of point A are:

$$X_A = a\sin\beta \tag{5.18}$$

$$Y_A = a\cos\alpha\cos\beta \tag{5.19}$$

$$Z_A = a\sin\alpha\cos\beta \tag{5.20}$$

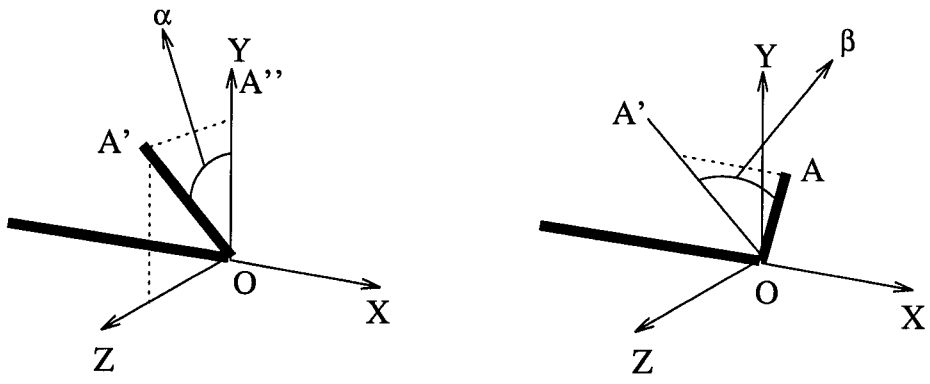

(a) Phase I
Point A moves from A'' to A'

(b) Phase II
Point A moves from A' to A

Figure 5.4: Two successive rotations of the coupler

Next, we can equate the coordinates of point A obtained in Eqs. (5.15), (5.16) and (5.17) with those Eqs. (5.18), (5.19) and (5.20). This results in the following three equations:

$$a \sin \beta = b(1 - \cos \theta) \tag{5.21}$$

$$a \cos \alpha \cos \beta = S \tag{5.22}$$

$$a \sin \alpha \cos \beta = b \sin \theta \tag{5.23}$$

Eq. (5.23) can be written as

$$a \cos \beta = b \frac{\sin \theta}{\sin \alpha} \tag{5.24}$$

Squaring and adding Eqs. (5.21) and (5.24) (to eliminate the terms containing β) results in

$$a^2 = b^2[(1 - \cos\theta)^2 + \frac{\sin^2\theta}{\sin^2\alpha}] \tag{5.25}$$

Eq. (5.25) can now be solved for θ in terms of the input angle α and the link lengths a and b. Dividing both sides of Eq. (5.25) by b^2 and replacing $\sin^2\theta$ by $(1 - \cos^2\theta)$, we get

$$a^2/b^2 = 1 - 2\cos\theta + \cos^2\theta + (1 - \cos^2\theta)/\sin^2\alpha \tag{5.26}$$

Eq. (5.26) can be written as a quadratic equation in $\cos\theta$ as

$$\cos^2\theta(\cos^2\alpha) + \cos\theta(2\sin^2\alpha) + (\frac{a^2}{b^2}\sin^2\alpha - \sin^2\alpha - 1) = 0 \tag{5.27}$$

Solving Eq. (5.27) for $\cos\theta$ we obtain

$$\cos\theta = \frac{-\sin^2\alpha \pm \sqrt{1 - \frac{a^2}{b^2}\cos^2\alpha\sin^2\alpha}}{\cos^2\alpha}, \text{ if } \cos\alpha \neq 0 \tag{5.28}$$

When $\cos\alpha = 0$, we have $\sin\alpha = \pm 1$ and Eq. (5.27) reduces to

$$\cos\theta = (1 - \frac{a^2}{2b^2}) \tag{5.29}$$

As a matter of fact, if we apply the limit when $\cos\alpha$ tends to zero to the Eq. (5.28), we get same result as in Eq. (5.29). So, finally we have the solution for θ as

$$\theta = \cos^{-1}[\frac{-\sin^2\alpha \pm \sqrt{1 - \frac{a^2}{b^2}\cos^2\alpha\sin^2\alpha}}{\cos^2\alpha}], \text{ if } \cos\alpha \neq 0 \tag{5.30}$$

and

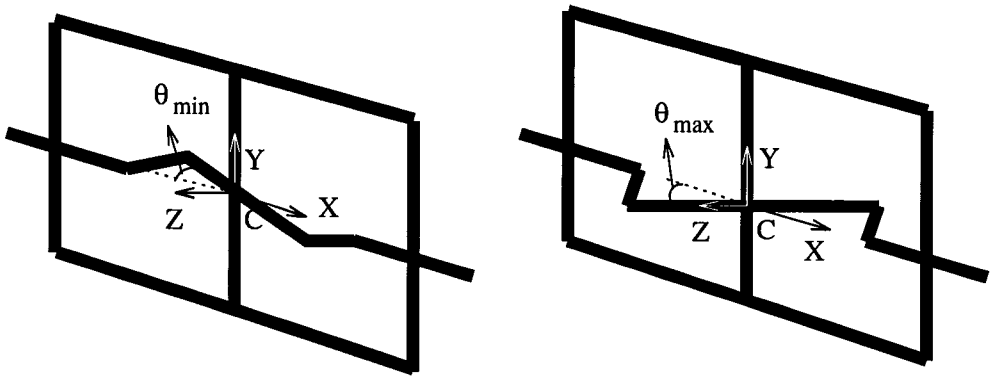

(a) Minimum θ position (b) Maximum θ position

Figure 5.5: Two extreme positions of the lever

$$\theta = \cos^{-1}(1 - \frac{a^2}{2b^2}), \text{ if } \cos\alpha = 0 \tag{5.31}$$

Eq. (5.30) implies that there are four different solutions of θ for each given α. However, we can prove that only two are feasible. To prove this, we first try to obtain the maximum and minimum values of θ as shown in Figure 5.5. Both the minimum and maximum values occur when the center of the lever reaches point C, where $\alpha = \pm 90$. For $\alpha = \pm 90$, Eq. (5.29) yields

$$\cos\theta_{max/min} = (1 - \frac{a^2}{2b^2}) \tag{5.32}$$

For $\theta_{max/min}$ to be real, the following condition must be met:

$$1 > 1 - \frac{a^2}{2b^2} > -1 \tag{5.33}$$

which yields

$$0 < \frac{a^2}{b^2} < 4 \tag{5.34}$$

Substituting Eq. (5.34) into Eq. (5.28) for the minus case of the equation yields

$$\cos\theta = \frac{-\sin^2\alpha - \sqrt{1 - \frac{a^2}{b^2}\cos^2\alpha\sin^2\alpha}}{\cos^2\alpha} < \frac{-\sin^2\alpha - \sqrt{1 - 4\cos^2\alpha\sin^2\alpha}}{\cos^2\alpha} \tag{5.35}$$

But the right-hand-side of Eq. (5.35) can be simplified as follows:

$$\frac{-\sin^2\alpha - \sqrt{1 - 4\cos^2\alpha\sin^2\alpha}}{\cos^2\alpha} = \frac{-\sin^2\alpha - \sqrt{1 - \sin^2 2\alpha}}{\cos^2\alpha} = -1 \tag{5.36}$$

Hence, Eq. (5.35) reduces to

$$\cos\theta < -1 \tag{5.37}$$

Eq. (5.35) implies that, for any value of $0 < \frac{a^2}{b^2} < 4$, the value of $\cos\theta$ would be less than –1. Hence, the minus sign in Eq. (5.28) is infeasible and the solution for θ reduces to

$$\cos\theta = \frac{-\sin^2\alpha + \sqrt{1 - \frac{a^2}{b^2}\cos^2\alpha\sin^2\alpha}}{\cos^2\alpha} \tag{5.38}$$

Eq. (5.38) yields two solutions of θ for a given value of α. That is if $\theta = \theta_o$ is a solution, then $\theta = -\theta_o$ is also a solution. Further, if $\theta = \theta_o$ yields a positive value of S, then $\theta = -\theta_o$ yields a negative value of S.

Once an expression for θ is obtained, we can get an expression for the position of the lever along its axis, S. Substituting $a\cos\beta$ from equation (5.24) into (5.22), we get

$$S = b\sin\theta\cot\alpha \tag{5.39}$$

Hence, there are two branches of solutions. For the mechanism to switch from one branch to another, the mechanism must be disassembled and then re-assembled.

5.1.2 Kinematic Analysis Using DADS

In this section, the kinematic analysis is performed in a more detailed manner using the software package DADS. Both the 1:-1 CV coupling (as in Figure 4.1) and the gearless differential mechanism (as in Figure 4.2) are simulated and the results are explained below.

(a) Kinematic Analysis of the Coupling

The mechanism is modelled as a real world system resembling (in its size) an existing differential gear box. The link lengths are chosen as $a = 3$ cm and $b = 6$ cm. For simplicity, all the links are assumed to be cylinders, their axes with respect to the global XYZ coordinate system at the instant shown in the Figure 5.6 is explained below. The local Y-axis of the input and output links are along the negative of the global X-axis, the local Y-axis of the couplers are along the global Y-axis and the local X-axis of the lever is along the global Y-axis. The term "world" in the Figure 5.6 represents the global coordinate system. The mechanism was driven at a constant angular velocity of 209.4 rad/s (2000 rpm), which was given as an input to the input link 2. The kinematic analysis resulted in the output link 6 rotating at the same speed but in the opposite direction of the input link 2, thus behaving as a 1:-1 CV shaft coupling.

As explained in the previous sections, one very important factor that affect the kinematics of the mechanism is the motion of the lever (middle link). The

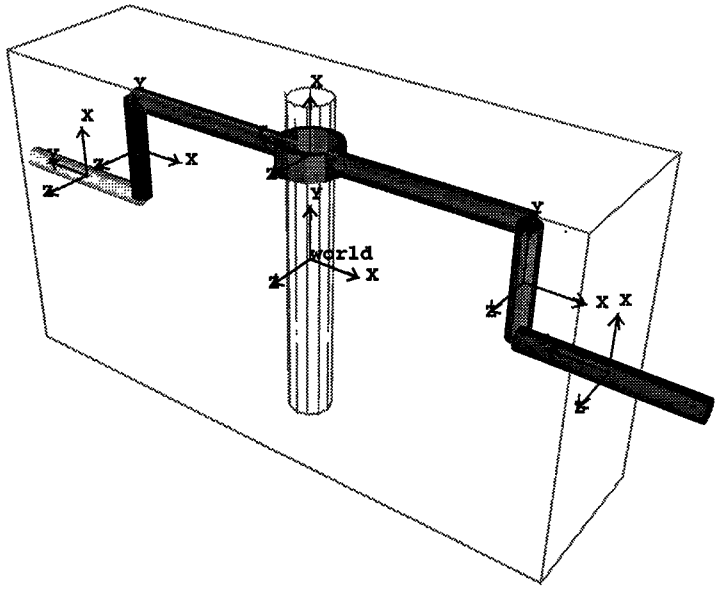

Figure 5.6: The model of a 1:-1 CV coupling

lever has motion only about the global Y-axis (both translation and rotation). For one rotation of the input shaft, the angular and linear displacements as well as velocities of the lever about the global Y-axis are plotted in Figs. 5.7 and 5.8. The displacements indicate that the lever oscillates ± 0.5 *rad* and slides ± 3 *cm*. The maximum angular velocity of the lever occurs at the top and bottom dead-center positions while the maximum linear velocity occurs at the mid-position of the lever, where the angular velocity is zero.

If we substitute the values of a and b into the Eq. (5.32), we get the same maximum and minimum values for the angular displacement of the lever as ± 0.5 *rad*.

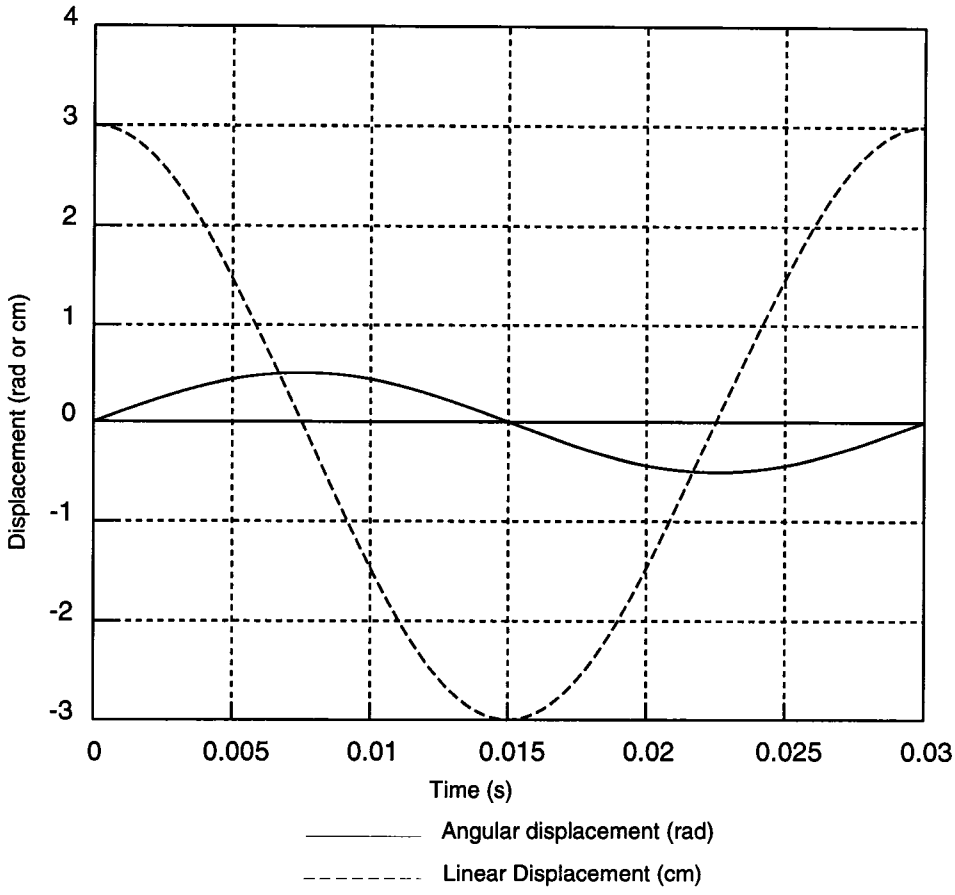

Figure 5.7: Angular and linear displacement of the lever

(b) Kinematic Analysis of the Gearless Differential

Now, the mechanism is simulated as a differential mechanism. The simulation model along with the global and local coordinate systems of the links are shown in Figure 5.9. The vehicle is assumed to move in a curve as shown in Figure 5.1 and the motion of the two output links (links 2 and 6) are analyzed when the cage (carrier) of the differential is driven at a constant angular velocity. The following values are inputted into the model:

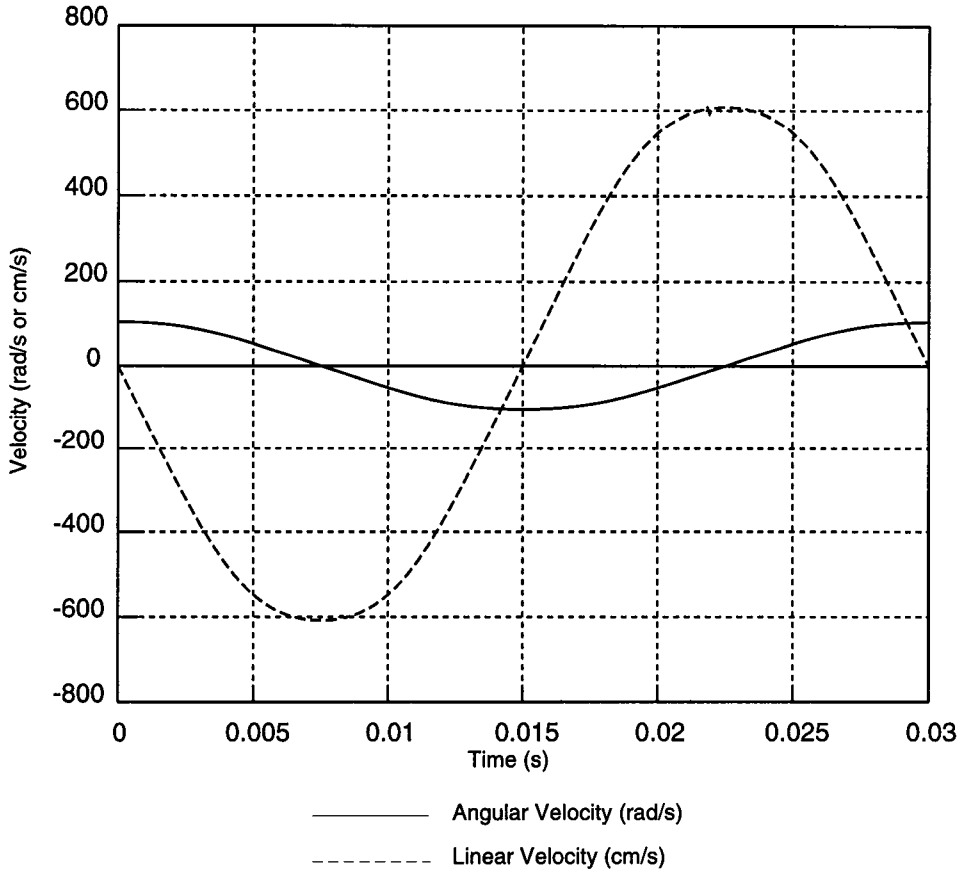

Figure 5.8: Angular and linear velocity of the lever

$a = 3\ cm$,

$b = 6\ cm$,

$R_{curve} = 700\ cm$,

$x = 140$ cm, and

$\omega_{cage} = 88\ rad/s$

During the simulation, it is observed that, for every ten revolutions of the input cage, the links inside the differential make one full cycle. This fact is clear when we notice that, for the above assumed values of R_{curve} and x, the differential

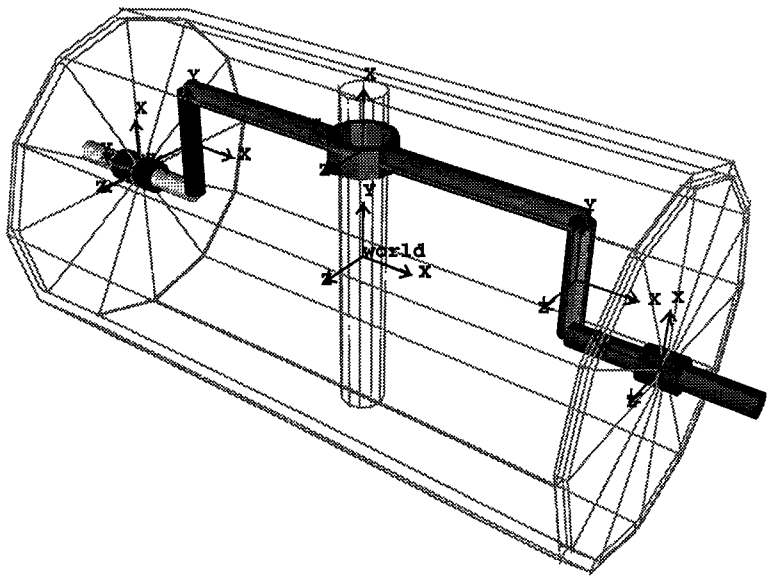

Figure 5.9: The model of a gearless differential mechanism

speed is one-tenth of the speed of the input cage which can be obtained from Eq. (5.12) (as $x/2R_{curve} = 0.1$).

The values of the angular velocities of the two wheels (links 2 and 6) along with the angular velocity of the cage are plotted in Figure 5.10. It is clear from Figure 5.10 that one of the wheels rotates faster than the other thus functioning as a differential mechanism in aiding the turn. It also confirms to Eqs. (5.13) and (5.14) in that, if we substitute the above values of R_{curve}, x and ω_{cage}, we get angular velocities of the wheels as 96.8 rad/s and 79.2 rad/s respectively.

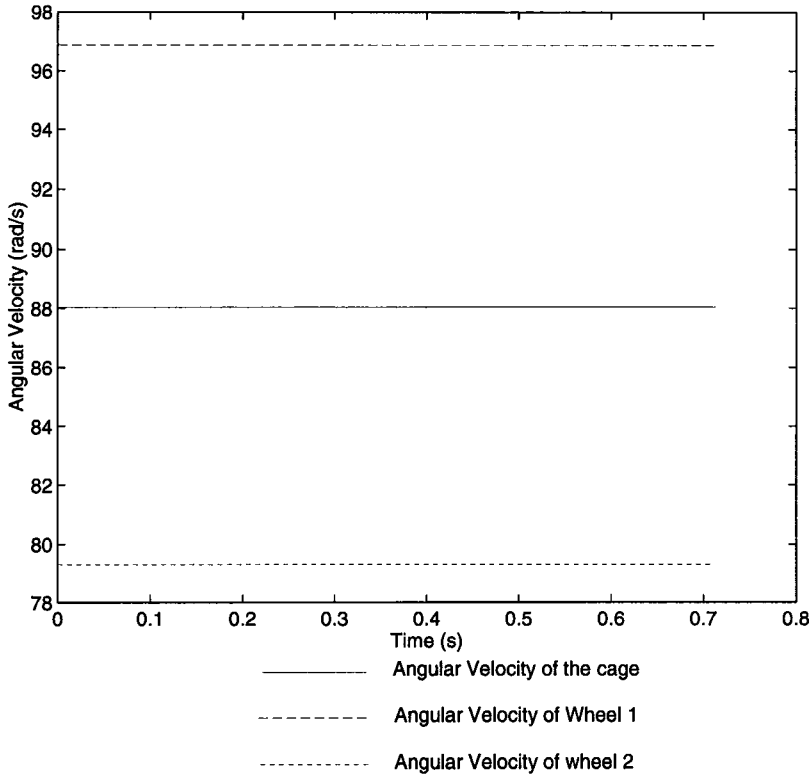

Figure 5.10: Angular velocities of the two wheels and the cage

5.2 Dynamic Analysis

In the previous sections, kinematic analysis was performed on the coupling and the gearless differential mechanism both analytically and using the software package DADS. In this section, a detailed dynamic analysis is performed on both the coupling and the gearless differential mechanisms and the results of the analysis are used to come up with some design guidelines for the design of a differential in the next chapter.

For the coupling, the input link 2 was given a constant angular velocity. For the differential, since it is a two degree-of-freedom mechanism, two inputs were given to the mechanism. One is for the cage of the differential and the other is

one of the output links 2. These inputs were calculated such that the vehicle will make a turn with a turning radius $R_{curve} = 700\ cm$, wheel base $x = 140\ cm$, and cage velocity $\omega_{cage} = 88\ rad/s$ as described in the previous section.

The gravitational effects are neglected as they are small and do not play an important role in a differential mechanism. The dynamic analysis of the differential is split into two sections. The first one considers the inertial effects with no external torques which is used to observe the shaking forces and moments on the ground link, while in the second section, external torques are applied to observe the forces and moments at the various joints.

The link lengths are chosen as the same values as that in kinematic analysis, i.e. $a = 3$ cm and $b = 6$ cm. The mass moment-of-inertias of all the links are calculated with respect to their local coordinate systems. Since all the links are assumed to be cylinders, the centers of mass of all the links are located at the centers of the cylinders which make the product of inertia, I_{xy}, I_{yz} and I_{xz} equal to zero for all the links. The mass and principal moment-of-inertia properties of the links are shown in Table 5.1. The details of these values are explained in Appendix A.

We note that the principal moments of inertia about all the three directions are left blank for the two output links. This is because, these values will never affect the dynamics of the mechanism. Since both the output links rotate about their fixed local Y-axes, the moments of inertia about the other two axes is not necessary for the model. Also, even the moments of inertia of the output links about their axis of rotation do not affect our model, since we are simulating only for the case of constant angular speeds of the wheels. So, even this component of moment-of-inertia is ignored. As a matter of fact, while performing the sim-

Table 5.1: Masses and moments of inertia

Link	*Mass* (g)	I_{xx} $(g.cm^2)$	I_{yy} $(g.cm^2)$	I_{zz} $(g.cm^2)$
Cage (Input)	4400	24200	93866.76	93866.67
Output1	20000	-	-	-
Coupler1	230	690	180	690
Lever	600	11250	468.75	11250
Coupler2	230	690	180	690
Output2	20000	-	-	-

ulation, this fact was verified by varying the values for the moment-of-inertia of the wheels and, as expected, it did not affect the dynamic results.

We also note that, when the mechanism is simulated as a coupling, the cage becomes the fixed link and so its mass and moment-of-inertia will have no consequence on the results of the simulation. But the above mentioned values for the cage in Table 5.1 does come into picture when the mechanism is simulated as a differential.

5.2.1 Dynamic Analysis of the Coupling

The mass properties given in Table 5.1 with the exception of the mass and moment-of-inertias of the cage are inputted into the model and dynamic analysis is performed. A constant angular velocity of 209.4 rad/s (2000 rpm) was given to the input link 2. The analysis gives us the forces and torques that are required to generate the prescribed motion and also the reaction forces and moments

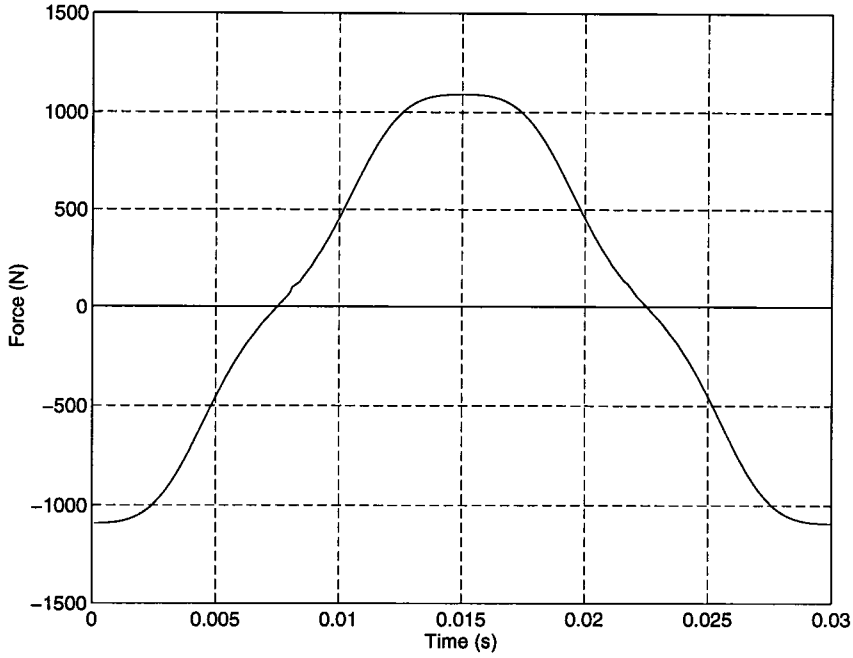

Figure 5.11: Shaking force about the global Y-axis (for the Coupling)

generated at the various joints and links. Also, no external torques are applied which implies that the main effects on the dynamics of the coupling will be the inertia effects.

An important factor to be considered in the dynamics of the coupling is the reaction forces and moments acting on the ground. These are better termed as the shaking forces and shaking moments due to the motion of the mechanism. The presence of symmetry in the mechanism yields no shaking forces and moments along the X and Z-axes. The shaking forces and moments acting on the carrier in the global Y-axis are shown in Figures 5.11 and 5.12 respectively.

We note that, when the mechanism is used as a differential, the differential speed would be quite small (in our simulation of the differential, $\omega_{diff} = 8.8$ rad/s) when compared to the speed at which the coupling is driven here (which

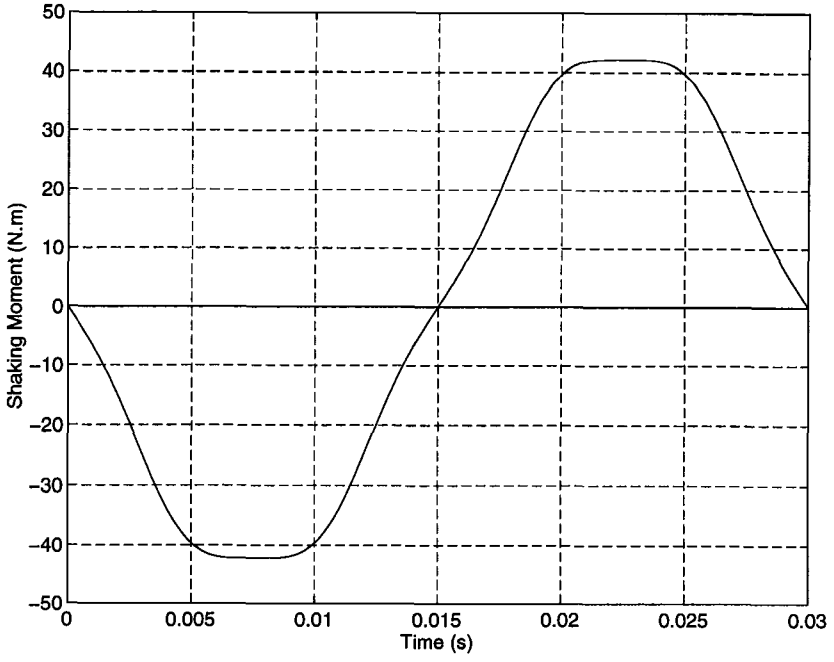

Figure 5.12: Shaking moment about the global Y-axis (for the Coupling)

is 209.4 rad/s). So, the shaking forces and moments should be much smaller for a differential than the values obtained in Figures 5.11 and 5.12 which will become clear from the simulation performed in the next section.

Another important factor to be considered in the dynamics of the coupling is the forces exerted on the lever at the C-pair. Since the lever can slide along and rotate about the axis of rotation of the C-pair (the global Y-axis) freely, there are no forces or moments exerted at the C-pair of the lever about this global Y-axis. The forces in the other two directions are plotted in Figures 5.13 and 5.14, respectively.

It is noted that the forces exerted on the lever at the C-pair is quite small. However, this will not be the case when external torques exist at the output shafts. The above plots, Figures 5.13 and 5.14, are shown just to prove the fact

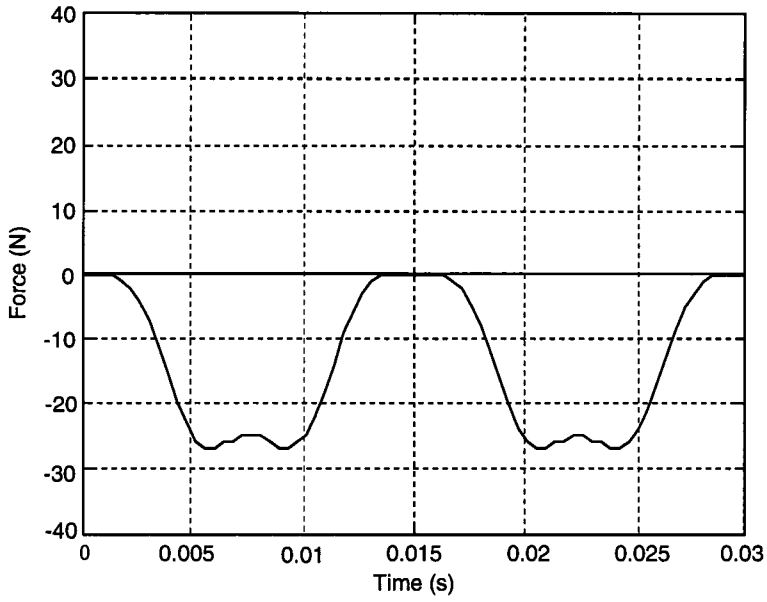

Figure 5.13: Force exerted on the lever at the C-pair along the global X-axis

that the effects of inertia forces at the joints are negligible when compared to the effects due to external torques. In the next section, when the dynamic analysis is performed on the differential, this fact will be proved.

5.2.2 Dynamic Analysis of the Gearless Differential

The dynamic analysis of the differential is split into two different parts. First, the inertia effects due to the motion of the links alone are considered, then the effects due to external torques at the wheels are considered. It will be shown that the effects due to inertia is much less when compared to the effects due to external torques.

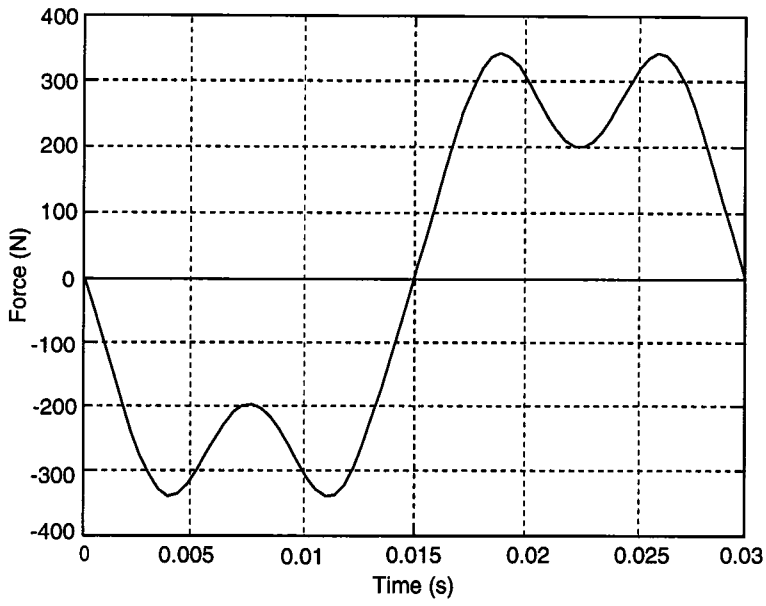

Figure 5.14: Force exerted on the lever at the C-pair along the global Z-axis

Inertia Effects

In this section, dynamic analysis is performed on the gearless differential using the mass and moment-of-inertias properties given in Table 5.1. A constant angular velocity of 88 rad/s was given to the cage (carrier), and the vehicle is assumed to be travelling in a curve whose radius of curvature, track width of the vehicle, and the link lengths are the same as that used for the kinematic analysis of the differential. The analysis gives us the forces and torques that are required to generate the prescribed motion and also the reaction forces and moments generated at the various joints.

Just as was the case with the coupling, an important factor to be considered in the dynamics of the differential is the shaking forces and moments acting on the ground. These play an important role especially for a differential since the differential will be mounted on a vehicle and too much shaking is undesirable.

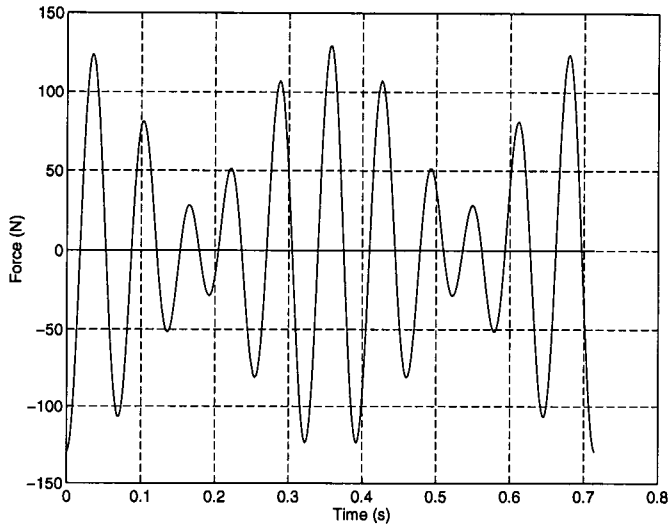

Figure 5.15: Shaking force along the global Y-axis

The analysis produces shaking forces and moments about the global Y and Z-axes as shown in Figures 5.15, 5.16, 5.17, and 5.18. The presence of symmetry in the mechanism about the global YZ plane yields no shaking forces and moments about the global X-axis.

There are a few important observations made from the plots obtained of the shaking forces for the differential. The first observation is that the shaking forces are not as high as that obtained for the 1:-1 CV coupling. This can be attributed to the fact that the differential speed of the mechanism is much slower than the speed of the coupling.

Another thing to be noted is the high number of peaks and valleys appearing in the curves obtained for the shaking forces and moments. This is attributed to the fact that the whole mechanism along with the cage is rotating about the axis of the wheels. As mentioned in the kinematic simulation of the differential, the cage makes ten revolutions for every cycle of differential motion. Since the whole

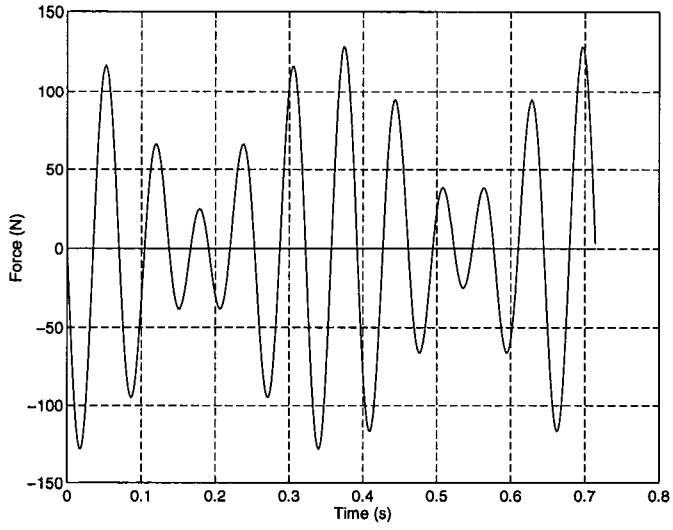

Figure 5.16: Shaking force along the global Z-axis

cage is rotating, the lever now not only slides and oscillates about its cylindrical axis but also rotates along with the cage about the global X-axis which generates centrifugal forces in the Y and Z-directions. This way, the inertia effect due to the rotation of the mechanism as a rigid body is modulated by that of the differential motion. The high frequency variation is due to the rotation of the cage and the low frequency variation is due to the differential motion.

Another interesting feature is noted when a comparison is made between the shaking forces generated in the differential and those generated in the coupling. The coupling exhibits no shaking forces and moments about the global X and Z-axes while the differential exhibits no shaking forces and moments about the global X-direction only. The presence of the forces in Z-direction of the differential can be attributed to the same fact that, the lever not only slides and oscillates about its axis but also rotates along with the cage about the global X-axis. All these factors illustrates the difference between the differential and

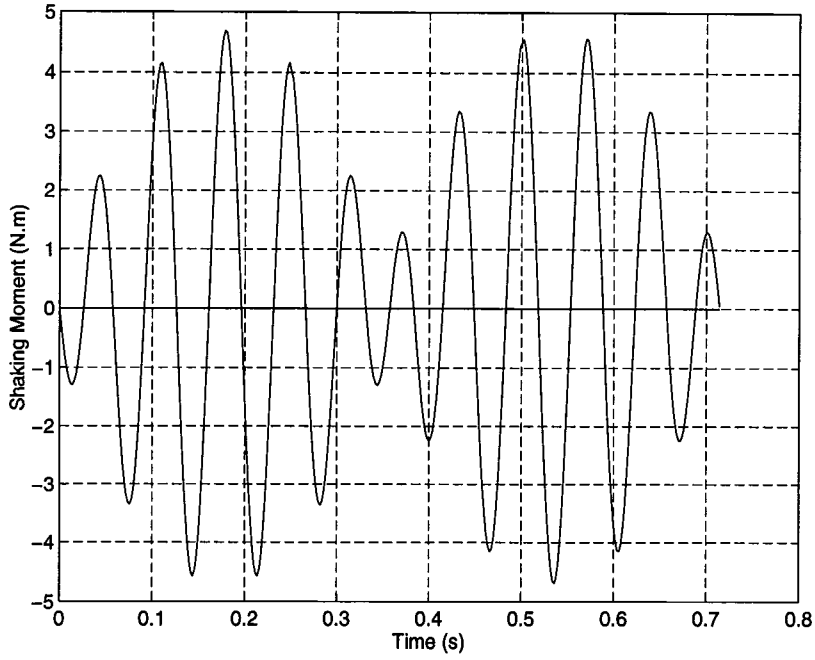

Figure 5.17: Shaking moment about the global Y-axis

the 1:-1 CV coupling.

Figure 5.19 shows the shaking force in the Y-axis versus the shaking force in the Z-axis. We can infer from Figure 5.19 as a rotating shaking force. At some instant in time, the shaking force points in the positive YZ quadrant, while at other instances, the shaking force points in the other three quadrants. For one full differential motion of the mechanism, the shaking force rotates, about the global X-axis, ten times with varying magnitude.

Effects Due to External Loads

In the previous section, we performed the dynamic analysis by applying a constant angular velocity to the cage and one of the output link 2, simulating the condition of a vehicle moving along a curve without any external loads. Hence,

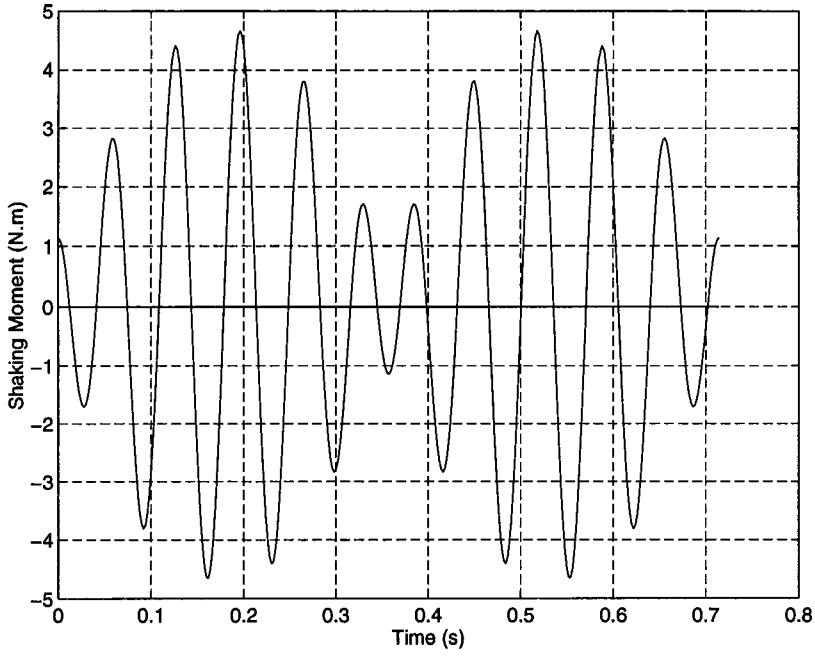

Figure 5.18: Shaking moment about the global Z-axis

the analysis gave us an idea about the nature of the inertia effects due to the moving links. However, in reality, this is not the case. For example, when a vehicle is cruising on a highway, there will be some input power supplied by the engine to the differential to overcome the external loads due to wind drag, friction between the tires and the ground, etc. These external loads act as external torques on the wheels and they must be accounted for the design of a differential.

To obtain expressions for these torques, a static analysis on the differential is performed. This analysis is very close to reality since the effects due to the external loads are quite high when compared to the inertial effects. Let

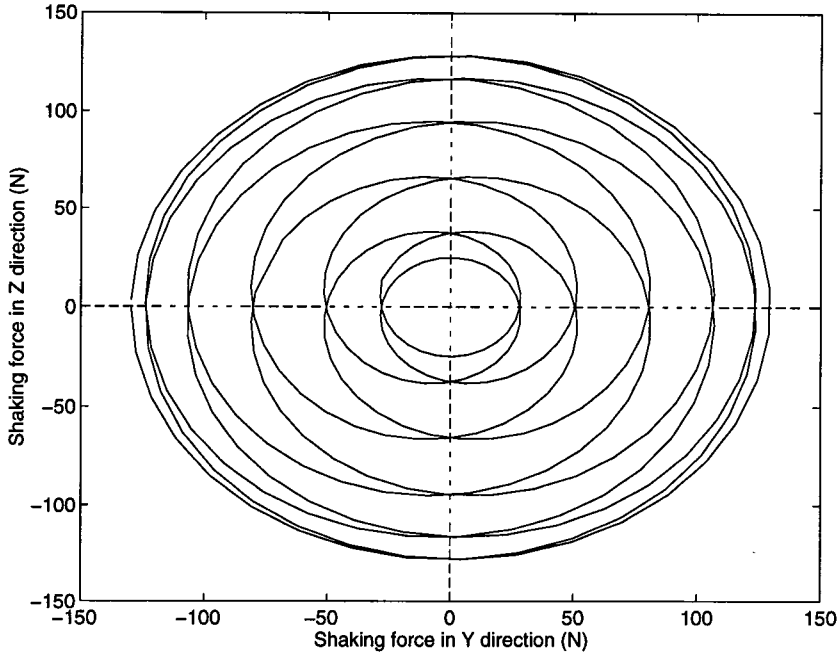

Figure 5.19: Shaking force in the Y-axis Versus Shaking force in the Z-axis

τ_{cage} be the input torque on the cage

τ_2, τ_6 be the external torques on the wheels

For the static analysis, we have

$$\tau_{cage} - \tau_2 - \tau_6 = 0 \tag{5.40}$$

If there is no loss of power inside the differential, then the input power must equate to the output power. That is

$$\tau_{cage}\omega_{cage} = \tau_2\omega_2 + \tau_6\omega_6 \tag{5.41}$$

Eqs. (5.40) and (5.41) can be used to solve for the torques on the wheels. From Eq. (5.40), we have

$$\tau_6 = \tau_{cage} - \tau_2 \tag{5.42}$$

From the section on kinematics (from Eqs. (5.1) and (5.2)), we have

$$\omega_6 = 2\omega_{cage} - \omega_2 \tag{5.43}$$

Substituting Eqs. (5.42) and (5.43) into Eq. (5.41), we get

$$\tau_2 = \tau_{cage}/2 \tag{5.44}$$

Hence, from Eqs. (5.42) and (5.44), we obtain an expression for τ_2 and τ_6 as

$$\tau_2 = \tau_6 = \frac{\tau_{cage}}{2} \tag{5.45}$$

From Eq. (5.45), we see that the external torques at the wheels are independent of the speed of rotation of the wheels and that they are always equal to one another (that is, $\tau_2 = \tau_6$) and equal to one half of the input torque. So, if one wheel rotates faster than the other (while taking a turn), more power is drawn by the faster rotating wheel in aiding the turn.

The above results are used to perform the dynamic analysis of the mechanism using DADS. The input power is approximately assumed to be 18 kW which is typical of a cruising speed. At this cruising condition, the cage of the differential is assumed to be rotating at a constant speed of 88 rad/s. So, we have

$$\tau_{cage} = \frac{18000}{88} \approx 200\ N.m \tag{5.46}$$

Hence, Eq. (5.45) yields

$$\tau_2 = \tau_6 = 100\ N.m \tag{5.47}$$

The vehicle is assumed to be making a turn with the same values of R_{curve} and x as those used for the kinematic analysis of the differential. To simulate the real world situation, the following approach is adopted. The input cage is driven at a constant angular velocity of 88 rad/s and link 2 is driven at a constant angular velocity as given by Eq. (5.13) of 96.8 rad/s. Also, an external torque $\tau_6 = 100\ N.m$ as given by Eq. (5.47) is applied to the other wheel (link 6). To prove that this does simulate the real world situation, we examine the driving torques that is necessary to kinematically drive the two inputs. The analysis was performed and we did notice that the two driving torques were $\tau_{cage} = 200\ N.m$ and $\tau_2 = 100\ N.m$ which correspond to Eqs. (5.46) and (5.47), respectively. It was also noted that the fluctuations in these driving torques (generated due to the inertial effects) were extremely small, thus proving our fact that the inertial effects are negligible when compared to the effects due to external torques.

The simulation was performed and a very important fact was noted from the results. The shaking forces and moments have the same values as those obtained in the previous section, where we considered only the inertial effects. This implies that the external torques exerted on the wheels, however large they are, do not have any effect on the shaking forces and moments. So, link inertias of the differential are responsible for producing those shaking forces and moments. But this is not the case for the forces exerted at the joints. The external torques has the largest effect on these forces while the inertia forces does not contribute much to the joint forces. This is discussed in more detail in

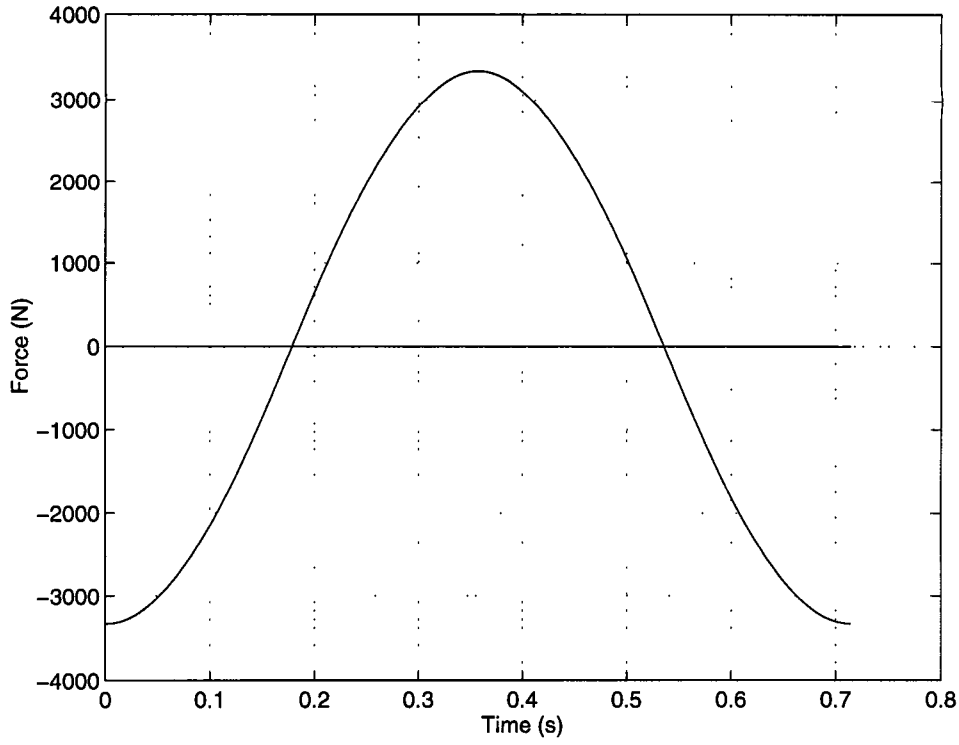

Figure 5.20: Forces acting on the lever at both the S-pairs along the local Z axis of the lever

the following paragraphs.

A few important force quantities are the forces exerted by the couplers on the lever about the local X and Z-axes of the lever. These forces are critical since they act at the spherical joints and the design of these joints are dependent on these forces. Also, since these are S-pairs, there will not be any moments at the joints. These forces exerted on the lever along the local Z-axis and the local X-axis of the lever are plotted in Figures 5.20 and 5.21, respectively.

Another important factor to be considered in the dynamics of the differential is the force and moment exerted on the lever by the cage at the C-pair. These are important since the size of the cylindrical joint depends on these forces and

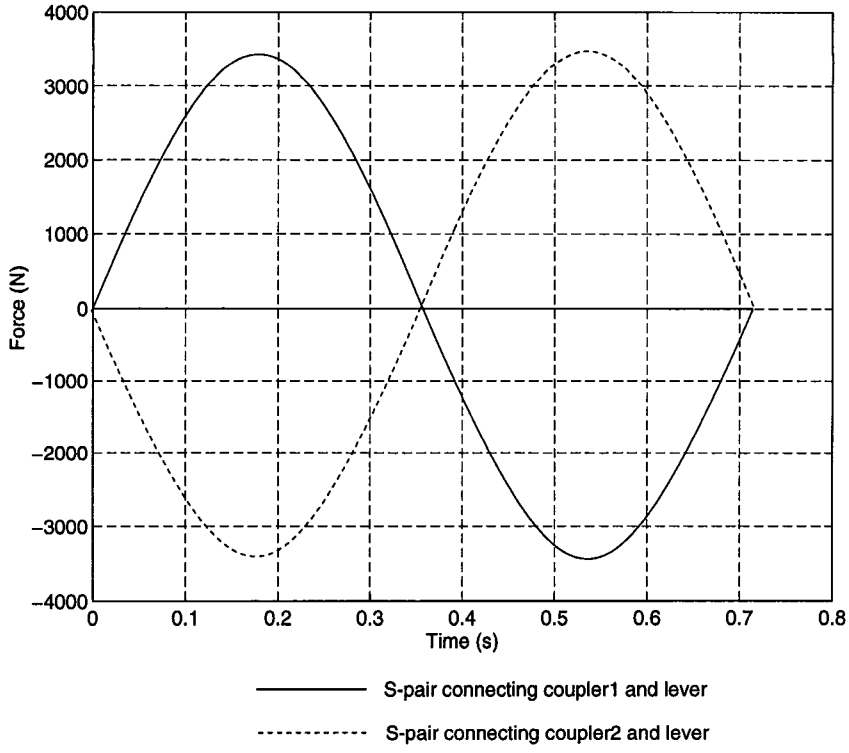

Figure 5.21: Forces acting on the lever at the S-pairs along the local X-axis of the lever

moments. Since the lever can slide along and rotate about the axis of rotation of the C-pair (the local X-axis of the lever) freely, there are no forces or moments exerted on the lever about its local X-axis. The force and the moment exerted on the lever at the C-pair about the local Z-axis of the lever are the important quantities to be considered. This becomes clear if we look at the free-body-diagram of the lever at any instant in time as shown in Figure 5.22.

The force along the local Z-axis of the lever, F_{zl2}, and the moment about the local Z-axis of the lever, M_{zl}, are plotted in Figures 5.23 and 5.24 respectively.

Considering the free-body-diagram of the lever as shown in Figure 5.22 and writing the force equilibirium equation and the moment equilibirium equation

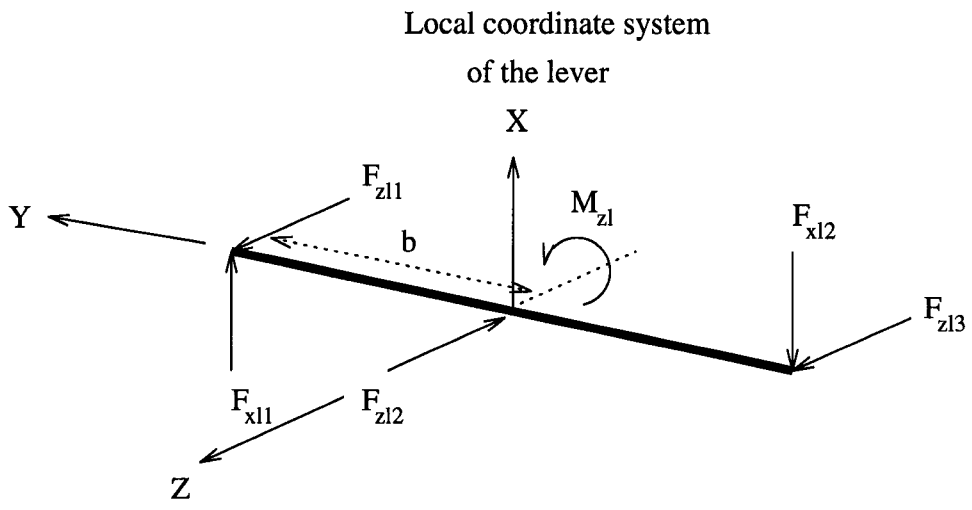

Figure 5.22: Free-body-diagram of the lever

along the local Z-axis of the lever, we have

$$F_{zl1} + F_{zl3} = F_{zl2} \tag{5.48}$$

and

$$M_{zl} = 2b(F_{xl1} + F_{xl2}) \tag{5.49}$$

Eqs. (5.48) and (5.49) are verified against the simulation data obtained, and they do agree with the data.

At the C-pair, there are equal and opposite forces and moments exerted on the cage. Since the lever slides freely along the local Y-axis of the cage, there are no forces and moments along the local Y-axis of the cage. But, forces and moments exist along the local X and Z-axes of the cage. At any instant in time, these forces and moments are drawn on the free-body-diagram of the cage as shown in Figure 5.25.

The force exerted on the cage at the C-pair along the local Z-axis and the

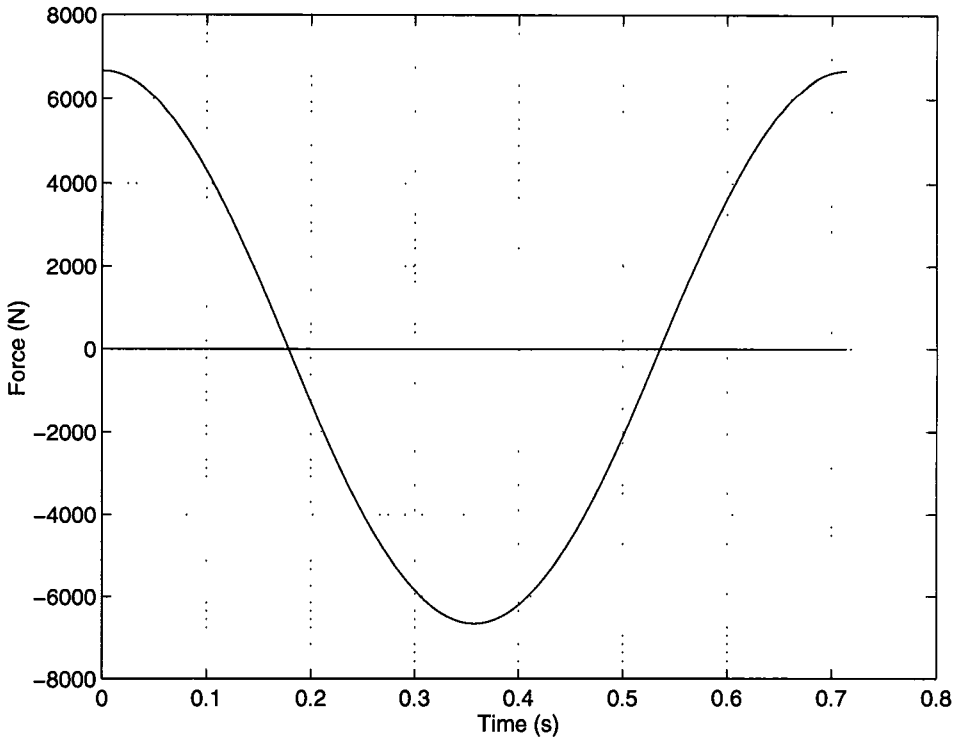

Figure 5.23: Force acting on the lever by the cage along the local Z-axis of the lever

moment exerted on the cage at the C-pair along the local X-axis are plotted in Figures 5.26 and 5.27, respectively.

Considering the free-body-diagram of the cage as shown in Figure 5.25 and writing the moment equilibirium equation about the local X-axis of the cage, we have

$$M_{xl} + F_{zl}S = \tau_{cage} = 200\ N.m \tag{5.50}$$

Eq. (5.50) is verified against the simulation data obtained, and it does agree with the data.

Figure 5.28 shows a plot of F_x versus F_z for the forces acting on the cage

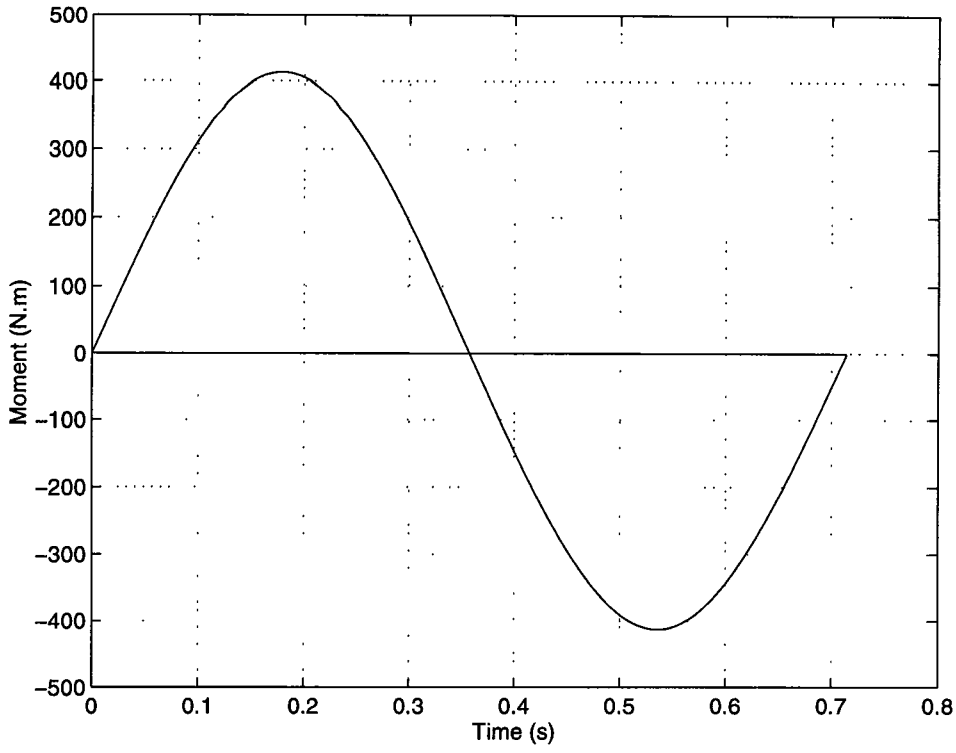

Figure 5.24: Moment acting on the lever by the cage about the local Z-axis of the lever

at the C-pair with respect to the local coordinate system of the cage. It shows that the direction of the force acting on the cage at the C-pair is continuously changing in magnitude and direction. This is good for the cylindrical joint as a rotating force permits better lubrication of the joint.

It was noted that the magnitude of the forces and moments at the joints due to the inertial effects were extremely small as compared to the effects due to the external torques. At the same time, it was also noted that the shaking forces and moments on the ground are due to the inertial effects only and that the external torques do not contribute in any way to the shaking forces and moments. In the next chapter, these results are used to come up with some design guidelines that

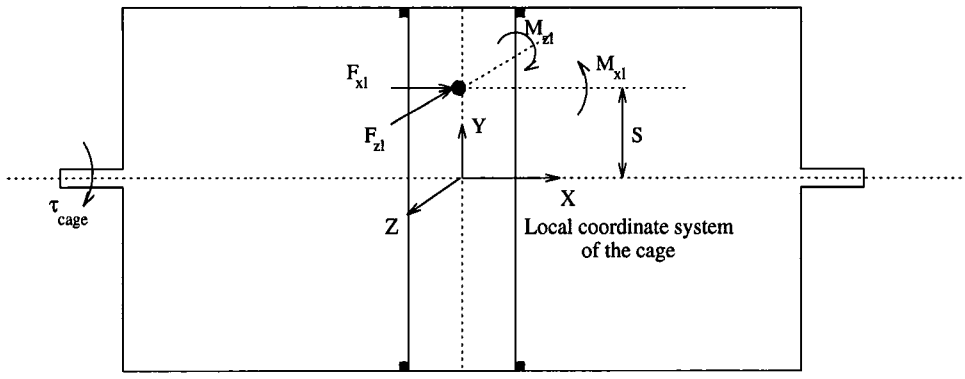

Figure 5.25: Free-body-diagram of the cage

can be used for the design of a gearless differential.

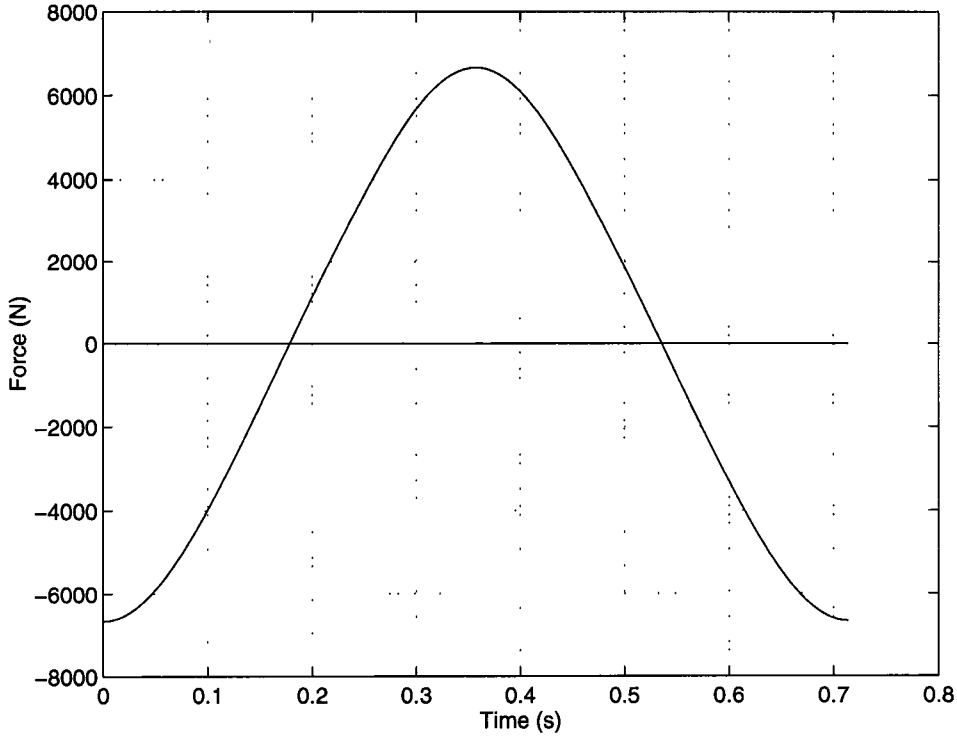

Figure 5.26: Force acting on the cage at the C-pair along the local Z-axis of the cage

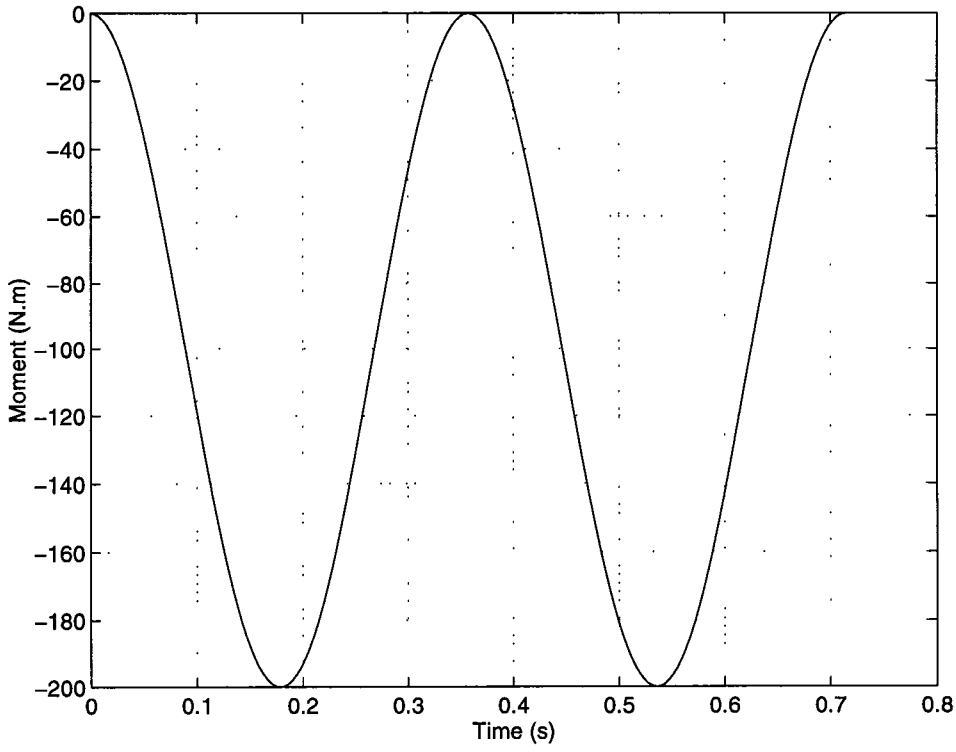

Figure 5.27: Moment acting on the cage at the C-pair about the local X-axis of the cage

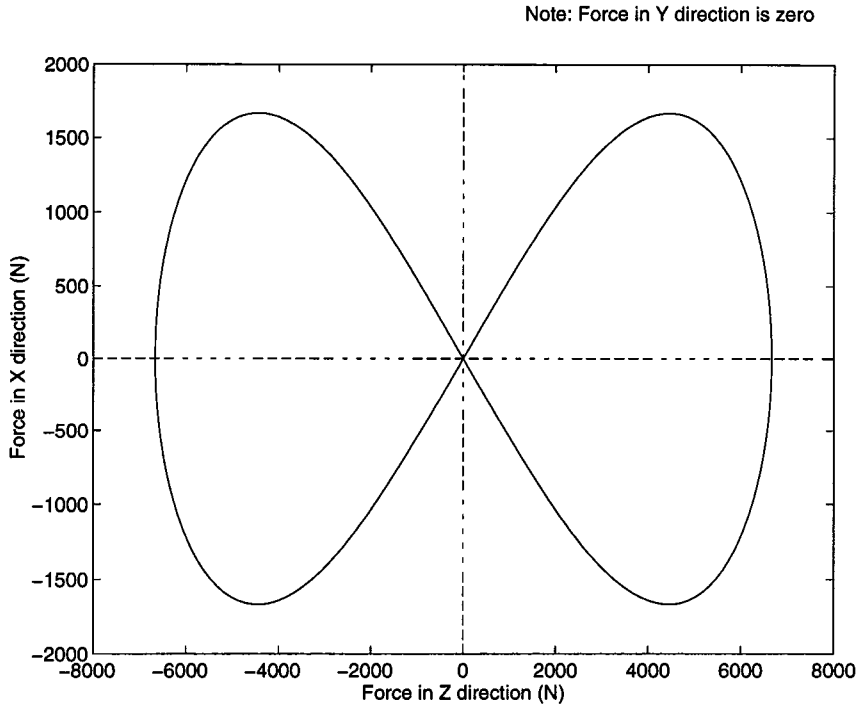

Figure 5.28: Forces acting on the cage at the C-pair about the local X-axis Versus the local Z-axis of the cage

Chapter 6

Design Guidelines

Based on the results from the previous chapter, we try to come up with some design rules that can be used to choose the link lengths for a differential. So, the aim of this chapter is to present some guidelines that can be adopted in choosing the link lengths, especially the values of a and b, of the mechanism. It is clear that, once the values of a and b are determined, it is just a matter of choosing the shapes of the links (for example, the diameter of a link) which will not affect the kinematics of the mechanism and is out of the scope of this work. The subsequent sections lay down these above mentioned design rules.

6.1 The Effect of a/b Ratio

From the kinematic analysis in the previous chapter, it is quite clear that the a/b ratio plays a very important role. This ratio appears on the equation that determines the orientation of the lever θ at any instant in time. The extreme values of θ is given by the Eq. (5.32):

$$\theta_{max/min} = \cos^{-1}\left(1 - \frac{a^2}{2b^2}\right) \tag{6.1}$$

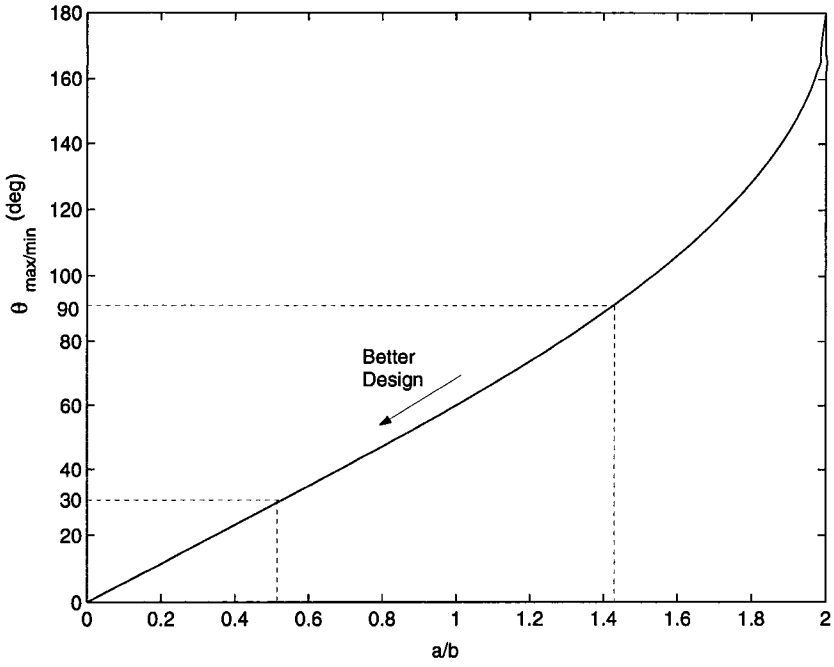

Figure 6.1: a/b versus $\theta_{max/min}$

Eq. (6.1) gives us a constraint on the a/b ratio (from Eq. (5.34)) as

$$0 < \frac{a}{b} < 2 \tag{6.2}$$

Let us look at how the a/b ratio affect the kinematics and dynamics of the mechanism. It is clear from Figure 6.1 that the oscillation angle of the lever increases with increasing a/b ratio. It is surely not advisable for the oscillation angles of the lever to go beyond ± 90 degrees as it would cause the two ends of the lever to cross the central YZ plane that splits the mechanism into two symmetric halves. As a matter of fact, larger the angle of oscillations of the lever, larger would be the angular velocities and accelerations of the lever. This implies the inertia effects will increase with the oscillation angle which in turn

will increase shaking forces and moments on the ground.

Hence, we can state that, for a better design, we prefer smaller values of the a/b ratio.

6.2 The effect of coupler link length (a)

Another factor to be considered is the amount of sliding of the lever along its cylindrical axis. The maximum value of this sliding, S_{max}, as given by Eq. (6.3), is equal to a (and S_{min} is, of course, $-a$). This value, as we can see, is independent of b.

$$S_{max} = a \tag{6.3}$$

It is clear from Eq. (6.3) that the sliding of the lever along its cylindrical axis will increase with increasing a. This implies that the linear velocity and acceleration of the lever along its cylindrical axis will increase with increasing value of a. So, the inertia and thus the shaking forces and moments on the ground will increase due to an increase in a.

Hence, we prefer the value of a to be small as this would decrease the sliding of the lever along its axis resulting in decreasing the inertia effects.

6.3 Suggested Values for the Link Lengths

In the previous sections, we have shown that the analysis favoured small a/b ratio as well as small value of a. First, a decision should be made as to how small the a/b ratio can we have. In our opinion, an angle of about 30 - 40 degrees of

oscillation of the lever about its cylindrical axis is a good choice. This is a design choice that a designer should make before sizing the actual link lengths. Next, the question arises as to why can't we further reduce the angle of oscillation? The reason is that, in reality, there will be torques acting on the two wheels, which will exert forces at the spherical joints connecting the couplers and the lever. If the value of a is very low, then the forces at the spherical joints would be very high due to the torques at the wheels. It will be inpossible to design spherical joints to withstand such high forces. This factor is considered in a later section and is explained in further detail there.

A value of $\theta_{max} = 30$ degrees was assumed and the link lengths are obtained. By substituting $\theta_{max} = 30$ degrees into Eq. (6.1), we obtain the a/b ratio as

$$\frac{a}{b} = 0.5176 \tag{6.4}$$

Once we have fixed a value for the a/b ratio, choosing the link lengths is just a matter of scaling the size of the mechanism. That is, if we increase the value of a, then correspondingly the value of b will increase to maintain the same a/b ratio thus making the mechanism size bigger. Next, a decision is made on the upper bound for the value of a. We see in the previous section that the lower the value of a is, the better it would be since the shaking forces and moments would decrease with a. In our opinion, a maximum value of the sliding of the lever (and thus on a) can be fixed at 3 cm. Based on this assumption, we have

$$a_{max} = 3\ cm \tag{6.5}$$

In all the constraints that have been laid out till now, we have considered only the effects due to the motion of the links which we know better as the inertial

effects. In the previous chapter on dynamics, we saw that the inertia effects affect mainly the shaking forces and moments on the ground but, in real world situation, there exists external torques on the wheels which is the major factor in generating various forces and moments at the various joints. The design of these joints depend on these forces and moments that they must withstand, and so, the effects due to the external torques on the wheels should be considered in laying out design guidelines for the differential mechanism. In the next section, we perform a parametric study by varying the values of a and b and keeping the a/b ratio constant as given by Eq. (6.4) and do the analysis with external torques as done in the second part of the dynamic analysis of the differential in the previous chapter.

6.4 Effect due to External Loads

The analysis, as done in the second part of the dynamic analysis of the differential, with the same input values for the external torques, is performed for different values of a and b while maintaining the a/b ratio constant given in Eq. (6.4). As mentioned in the previous chapter, the reaction force at the spherical joint is an important criterion in design since this force decides the size of the spherical joint. It is clear that the spherical joint must withstand this force and so a smaller force is preferred. The maximum resultant force at the spherical joint during one full differential motion is plotted as a function of a as shown in Figure 6.2.

Figure 6.2 was plotted as follows. First, the magnitude of the force exerted at the spherical joint is plotted as a function of time for one full differential motion

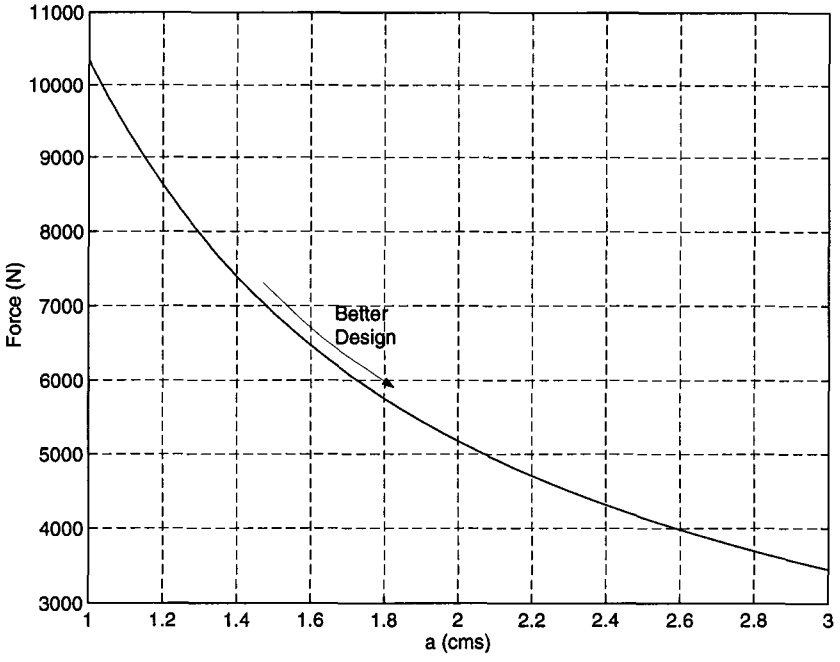

Figure 6.2: Maximum force at the spherical joint Versus the value of a

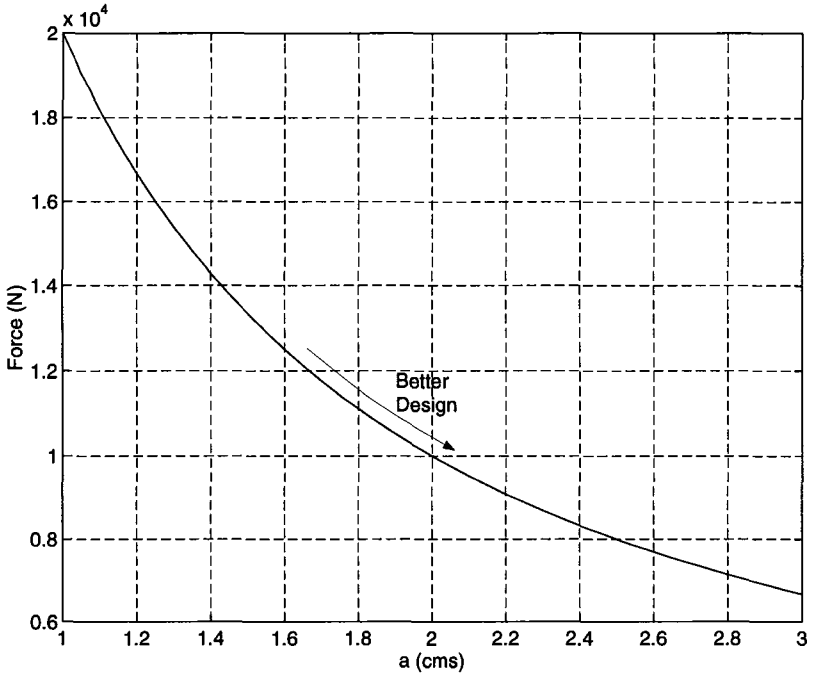

Figure 6.3: Maximum force at the cylindrical joint Versus the value of a

(which is equivalent to ten revolutions of the cage as shown in the previous chapter) and for a given value of a. Then, the maximum force is identified for that particular plot. The process is repeated for different values of a and the result is plotted in Figure 6.2.

It is clear from Figure 6.2 that, as a increases, the force exerted at the spherical joint will decrease. Since we prefer this force be as small as possible, we need to go for higher values of a. But the maximum value on a is limited by the Eq. (6.5). So, we can choose our value of a as

$$a = 3\ cm \tag{6.6}$$

Next, the maximum resultant force at the cylindrical joint is for one full

differential motion is plotted as a function of a as shown in Figure 6.3. Figure 6.3 was plotted in the same manner as Figure 6.2. Again from Figure 6.3, we note that, for the force at the cylindrical joint to be small, we need to go for higher values of a. So, from the point of view of the cylindrical joint too, we can choose the value of a to be 3 cm as given by Eq. (6.6).

Substituting Eq. (6.6) into Eq. (6.4), we have the value of b as

$$b = 5.8\ cm \tag{6.7}$$

From the discussion so far, we can come to the following conclusions. Smaller values of a and b are preferred as they reduce the inertia effects and thus the shaking forces and the moments on the ground. But, at the same time, due to the external torques acting on the wheels, we prefer larger value of a as this reduces the forces acting at the spherical and the cylindrical joints which is an important criterion in the design of these joints. Hence, both facts must be considered for obtaining optimal link lengths. In the above discussion, we did consider both these facts for designing the link lengths and the values we obtained are given by Eqs. (6.6) and (6.7).

Chapter 7

Conclusion and Future Study

7.1 Conclusion

We have adopted an improved methodology for the enumeration of all possible gearless differential mechanisms which satisfy a set of search specifications. The method adopted here was to first enumerate 1:-1 constant-velocity shaft couplings which are later transformed into gearless differentials. First, the functional requirements of a 1:-1 CV shaft coupling which is suitable for application as a gearless differential are defined. Then, most of these functional requirements are translated into structural characteristics and incorporated in a generator for the enumeration of mechanism structures. The remaining functional requirements are implemented in a tester for the evaluation of mechanism structures. As a result, we obtain four potential 1:-1 CV shaft couplings and thus four potential gearless differentials..

To perform a feasibility study, a promising candidate mechanism is chosen for the kinematic and dynamic analysis. The analysis is performed on both the 1:-1 CV shaft coupling and the differential. The analysis reveals that the 1:-1

CV coupling can provide a 1:-1 velocity ratio between the input and the output shafts. Also, the differential mechanism does have the capability in providing the differential motion that is necessary for a vehicle to make a turn. The mechanism was simulated by using the DADS software package and the differential motion was observed on the simulated results.

The lever link in the differential possesses a continuous sinusoidal motion. Due to this continuous motion, the singularity condition is avoided. The rotation of the lever is out of phase with respect to its translation by 90 degrees and the shaking force and moment acting on the ground are negligibly small. The joint reaction forces and moments are sinusoidal and reasonably small for a common bearing size. We can conclude that the mechanism does have the potential for application as a gearless differential as well as a 1:-1 CV coupling. Finally, design guidelines which can be used to obtain optimal values for the link lengths were established.

7.2 Future Study

The dynamic analysis was performed only for the case of a vehicle at a cruising speed. Another important case that must be studied is the case when the vehicle is accelerating. When the vehicle is accelerating, the ground reaction torques at the wheels will increase significantly. This is important since the joint reaction forces and moments depend primarily on the external loads.

Also, one can try to derive the dynamic equations that govern the motion of the differential. Once these equations are obtained, one can solve the problem of design as a multi-objective optimization problem, with the objectives of

minimizing the shaking forces and moments on the ground and minimizing the forces and moments at the joints.

As a further part of future study, a prototype mechanism can be developed using the optimal link lengths to establish a proof of the concept. Also, we can perform a detailed finite element stress analysis on the links by using one of the many available FEM packages. This will give a further insight on the performance on the differential.

The following section presents an alternate approach for the design of the differential mechanism.

7.3 An alternate design

In this section, a different approach for the design of the differential mechanism is presented. This involves the positioning of the couplers in a slightly different way. In the previous design, (from Figure 5.3) we have chosen $\beta = 0$ when $\alpha = 0$ such that the couplers are perpendicular to the axis of the output shafts. This way, β goes from 0 to β_{max} as the lever oscillates.

In this section, we modify the approach slightly such that $\beta \approx -\beta_{max}/2$ when $\alpha = 0$ and 180 deg and $\beta \approx \beta_{max}/2$ when $\alpha = 90$ and 270 deg.

This is clearly shown in Figure 7.1. A comparison of the values of β of the new approach with the previous design is sketched in Table 7.1.

We can see from this comparison that the coupler oscillates between $\beta \approx -\beta_{max}/2$ and $\beta \approx +\beta_{max}/2$ for the new design, while for the previous design, it oscillates between $\beta = 0$ and $\beta = \beta_{max}$. This design has an advantage with respect to the force exerted at the spherical joints.

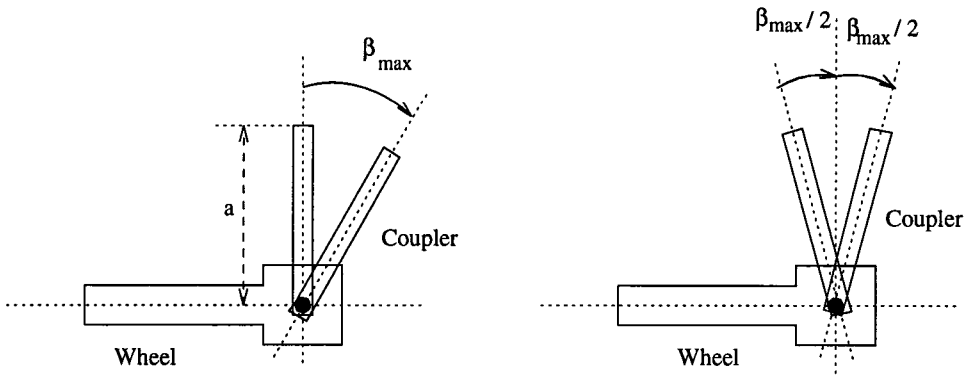

(a) Previous design

(b) Alternate design

Figure 7.1: Oscillations of the coupler

If we assume an external torque τ_2 is acting on link 2, then the force, F_s, exerted at the sperical joint due to this torque is given as

$$F_s = \frac{\tau_2}{a \cos \beta} \tag{7.1}$$

It is clear from Eq. (7.1) that F_s is maximum when β attains its maximum value. In the new design, the maximum value of β would be approximately equal to one-half of the previous design. Hence, the maximum force at the spherical joints due to the external torques is reduced. This is a nice improvement and is recommended for future study.

Table 7.1: Comparison of approximate values of β

α	β Previous design	β New design
0	0	$-\beta_{max}/2$
90	β_{max}	$\beta_{max}/2$
180	0	$-\beta_{max}/2$
270	β_{max}	$\beta_{max}/2$
360	0	$-\beta_{max}/2$

Appendix A

Velocities of the center of the two wheels for a vehicle moving in a curved path

In this section, the velocities of the centers of the two wheels at any instant are derived when the vehicle is assumed to be moving in a curved path as shown in Figure A.1. These velocities are obtained as a function of the velocity of the center of the cage, the instantaneous radius of curvature and the distance between the two wheels of the vehicle. The velocities obtained here are used in Eqs. (5.3) and (5.4) for the kinematic analysis.

In Figure A.1, let

V_0	:	velocity of the center of the cage with respect to the ground
V_2, V_6	:	velocities of the centers of the two wheels with respect to the ground
x	:	distance between the two wheels of the vehicle
R_{curve}	:	instantaneous radius of curvature of the curved path
$\hat{i}, \hat{j}, \hat{k}$	:	orthogonal unit vectors fixed to the ground
$\hat{n_1}, \hat{n_2}$	:	orthogonal unit vectors fixed on the chassis of the vehicle

The unit vector $\hat{k}$ is perpendicular to the ground and the unit vectors $\hat{i}$ and $\hat{j}$ are in the plane of the ground. While the unit vectors $\hat{i}$, $\hat{j}$ and $\hat{k}$ are fixed on the ground, the unit vectors $\hat{n_1}$ and $\hat{n_2}$ are fixed on the chassis of the vehicle. So, these two vectors move along with the vehicle and keep changing directions as the vehicle moves in a curved path. At the instant of time shown in Figure A.1, O is the instantaneous center of rotation about which the whole vehicle can be assumed to be rotating.

At the instant shown in Figure A.1, the velocity of the center of the cage, V_0 is given by

$$\vec{V_0} = \dot{\theta}\hat{k} \times R_{curve}\hat{n_1} \tag{A.1}$$

where $\dot{\theta} = \frac{d\theta}{dt}$, represents the rate of change of rotation of the vehicle about the instantaneous center of rotation with respect to the ground.

This gives

$$\vec{V_0} = \dot{\theta}R_{curve}\hat{n_2} \tag{A.2}$$

Similarly, we obtain the velocities of the centers of the two wheels as

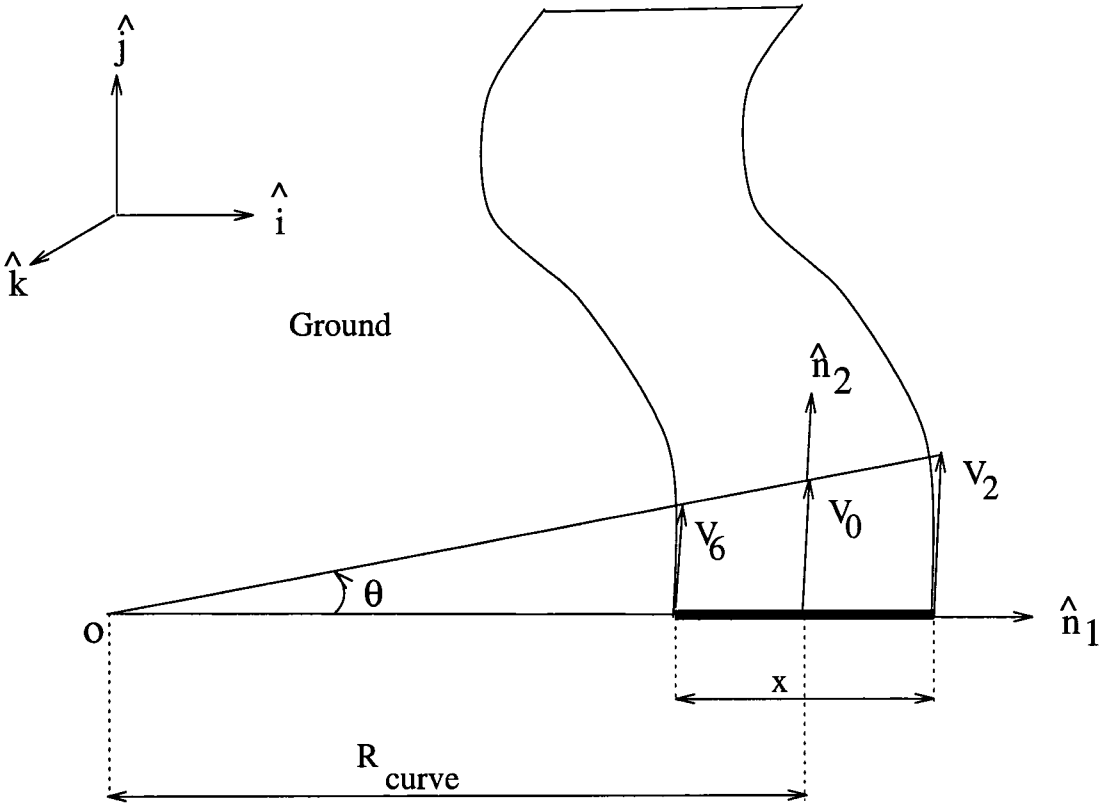

Figure A.1: Vehicle moving in a curved path

$$\vec{V_2} = \dot{\theta}\hat{k} \times (R_{curve} + x/2)\hat{n_1} \tag{A.3}$$

which gives

$$\vec{V_2} = \dot{\theta}(R_{curve} + x/2)\hat{n_2} \tag{A.4}$$

and

$$\vec{V_6} = \dot{\theta}\hat{k} \times (R_{curve} - x/2)\hat{n_1} \tag{A.5}$$

which gives

$$\vec{V_6} = \dot{\theta}(R_{curve} - x/2)\hat{n_2} \tag{A.6}$$

Just considering the magnitude of the velocities in Eqs. (A.2), (A.4) and (A.6) and eliminating $\dot{\theta}$, we obtain

$$V_2 = V_0 \frac{(R_{curve} + x/2)}{R_{curve}} \tag{A.7}$$

and

$$V_6 = V_0 \frac{(R_{curve} - x/2)}{R_{curve}} \tag{A.8}$$

Eqs. (A.7) and (A.8) are used in Eqs. (5.3) and (5.4) and the kinematic analysis is performed.

Appendix B

Moments-Of-Inertia of Various Links

In this section, we explain as to how we obtained the values of the moments of inertia for the various links in the mechanism. As mentioned in the dynamic analysis, all the links were assumed to be cylinders which resulted in zero product-of-inertia for all the links. Also, in the section of dynamic analysis, reasons were given for neglecting the moments of inertia of the wheels. Now, we consider all the other links, one by one, and evaluate their masses and principal moment-of-inertia properties.

To obtain the mass of the links, we assume all the links are made out of steel whose density equals 7.9 g/cm^3. We calculate the volumes of each link and multiply it by the density of steel to obtain the mass. To obtain the principal moments of inertia, we assume all the links except the cage as solid cylinders and the cage to be a hollow cylinder.

For any solid cylinder as shown in Figure B.1 along with a center-of-mass coordinate system, we have

$$I_{xx} = \frac{mr^2}{2} \tag{B.1}$$

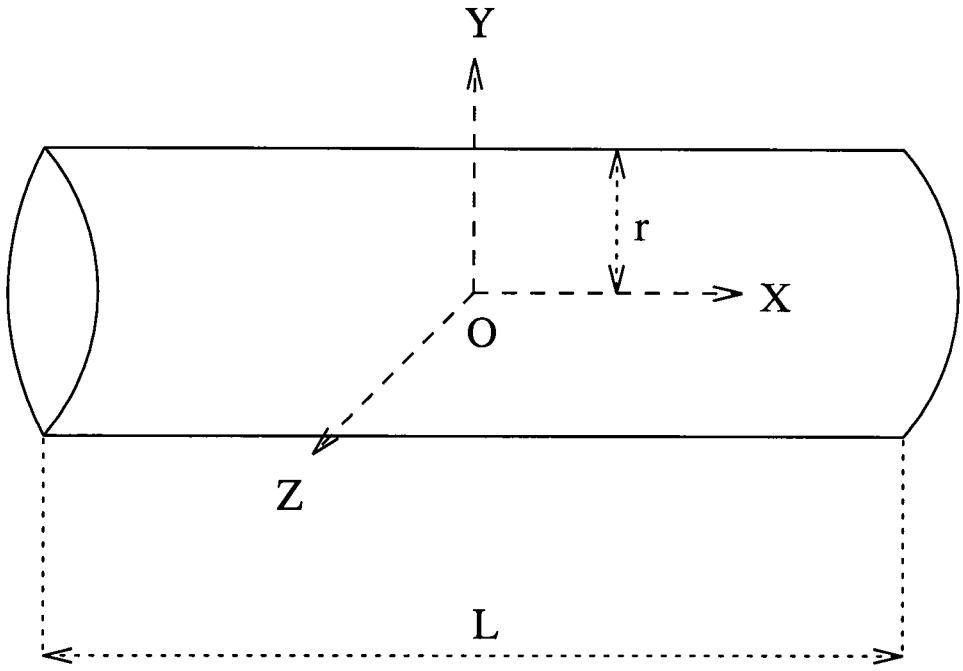

Figure B.1: Moment-of-inertia of a cylinder

$$I_{yy} = \frac{mL^2}{12} \tag{B.2}$$

$$I_{zz} = \frac{mL^2}{12} \tag{B.3}$$

and for a hollow cylinder, we have

$$I_{xx} = \frac{m(r_2^2 - r_1^2)}{2} \tag{B.4}$$

$$I_{yy} = \frac{mL^2}{12} \tag{B.5}$$

$$I_{zz} = \frac{mL^2}{12} \tag{B.6}$$

where r_2 and r_1 are the outer and inner radius of the hollow cylinder respectively, m is the mass of the cylinder and L is the length of the cylinder.

In our model, we needed to supply to moments-of-inertia of a body with respect to its center-of-mass coordinate system. In the coming sections, we evaluate the moments-of-inertia of the various links with respect to their center-of-mass coordinate systems.

B.1 Couplers

Figure B.2 shows the coupler along with its center-of-mass coordinate system and the length and diameter of the body. Points A and B in the Figure B.2 show the places where the R and the S-pairs are located, and the distance between A and B equals 3 *cm*.

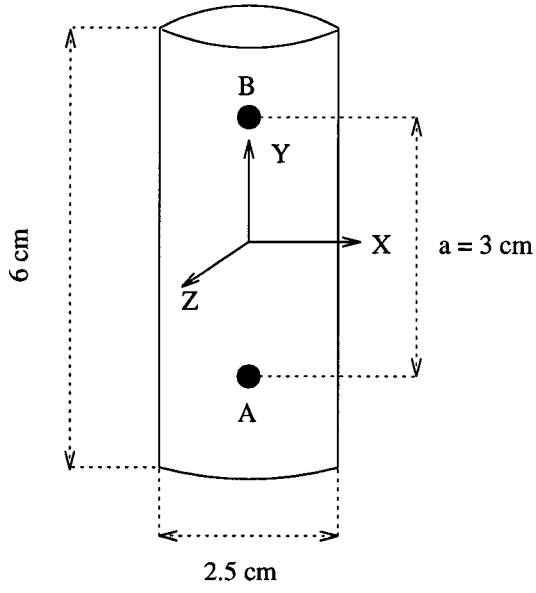

Figure B.2: Coupler

The length and radius of the coupler along with the density of steel gives us

the mass of the coupler as approximately 230 g. Since the local Y-axis of the coupler is along the axis of the cylinder, we obtain $I_{yy} = \frac{mr^2}{2} \approx 180\ g.cm^2$ and $I_{xx} = I_{zz} = \frac{mL^2}{12} \approx 690\ g.cm^2$.

B.2 Lever

Figure B.3 shows the lever along with its center-of-mass coordinate system and the length and diameter of the body. Points A, B and C in the Figure B.2 show the places where the left S, C and the right S pairs are located, and the distance between A and B equals 6 cm.

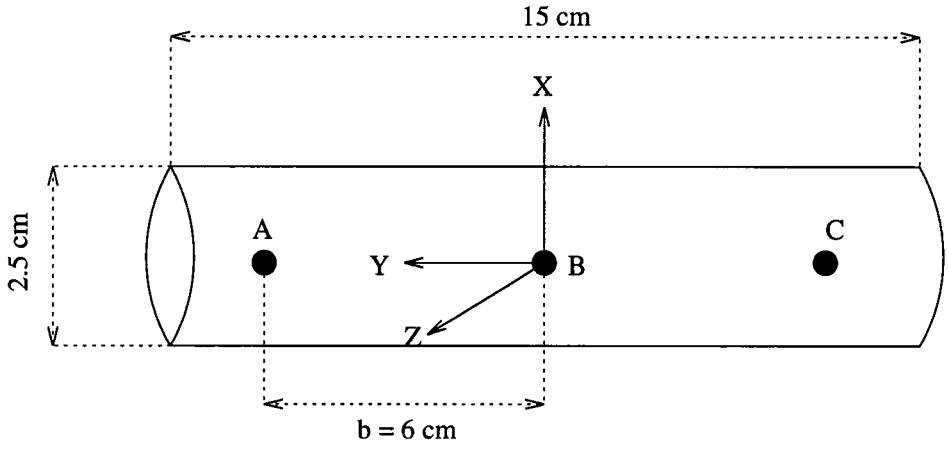

Figure B.3: Lever

The length and radius of the lever along with the density of steel gives us the mass of the lever as approximately 600 g. Since the local Y-axis of the lever is along the axis of the cylinder, we obtain $I_{yy} = \frac{mr^2}{2} \approx 468.75\ g.cm^2$ and $I_{xx} = I_{zz} = \frac{mL^2}{12} \approx 11250\ g.cm^2$.

B.3 Cage

The cage is assumed to be a hollow cylinder as shown in Figure B.4 along with its center-of-mass coordinate system.

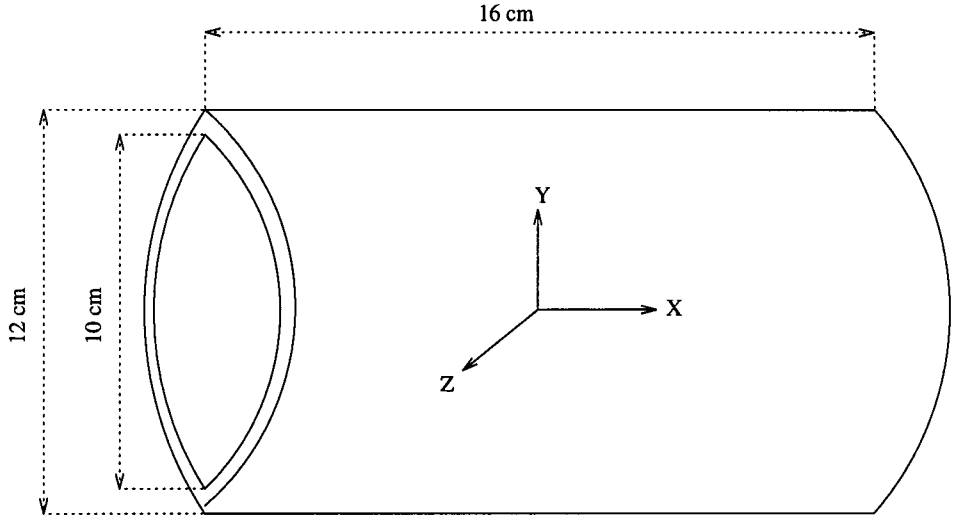

Figure B.4: Cage

The length and the inner and outer radii of the cage along with the density of steel gives us the mass of the cage as approximately 4400 g. Since the local X-axis of the cage is along the axis of the cylinder, we obtain $I_{xx} = \frac{m(r_2^2 - r_1^2)}{2} \approx 24200$ $g.cm^2$ and $I_{yy} = I_{zz} = \frac{mL^2}{12} \approx 93866.67$ $g.cm^2$.

Bibliography

[1] CADSI, 1993, "DADS User's Manual," Revision 7.6, *Computer Aided Design Software, Inc.,* Coralville, Iowa.

[2] Chatterjee, G., and Tsai, L.-W., 1994a "Enumeration of Epicyclic-Type Automatic Transmission Gear Trains," SAE Paper No. 941012, SAE 1994 Transactions, Vol. 103, Sec. 6, pp. 1415-1426.

[3] Chatterjee, G., and Tsai, L.-W., 1994b "Computer-Aided Sketching of Epicyclic Type Automatic Transmission Gear Trains," *Proceedings of the ASME 1994 Design Technical Conferences*, DE-Vol. 71, Machine Elements and Machine Dynamics, pp. 275-282.

[4] Dobrjanskyj, L., and Freudenstein, F., 1967, "Some Applications of Graph Theory to the Structural Analysis of Mechanisms," *ASME Journal of Engineering for Industry,* Vol. 89, pp. 153-158

[5] Freudenstein, F., and Maki, E.R., 1979, "The Creation of Mechanisms According to Kinematic Structure and Function," *Journal of Environment and Planning B*, Pergamom Press, Vol. 6, pp. 375-391.

[6] Freudenstein, and F., Maki, E.R., 1983, "Development of an Optimum Variable-Stroke Internal-Combustion Engine Mechanism from the Viewpoint

of Kinematic Structure," ASME *Journal of Mechanisms, Transmissions and Automation in Design,* Vol. 105, pp. 259-266.

[7] Freudenstein, F., and Maki, E.R., 1984, "Kinematic Structure of Mechanisms for Fixed and Variable-Stroke Axial-Piston Reciprocating Machines," ASME *Journal of Mechanisms, Transmissions and Automation in Design,* Vol. 106, No. 3, pp. 355-364.

[8] Habil, I., and Altmann, F.G., 1950, "Coupler Transmissions for Uniform Transmission Ratio," *Association of German Engineers, Braunschweig.*

[9] Hunt, K.H., 1973, "Constant-Velocity Shaft Couplings: A General Theory," ASME *Journal of Engineering for Industry,* 95B, pp. 455-464.

[10] Mavroidis, C., and Roth, B., 1995a, "Analysis of Overconstrained Mechanisms," ASME *Journal of Mechanical Design,* Vol. 117, No. 1, pp. 69-74.

[11] Mavroidis, C., and Roth, B., 1995b, "New and Revised Overconstrained Mechanisms," ASME *Journal of Mechanical Design,* Vol. 117, No. 1, pp. 75-82.

[12] Moore, and J.W., Greenwood, D.G., 1994, "The Ricardo Differential," *The Ricardo Consulting Engineers Ltd.,* Technical Report DP 94/0229, West Sussex, UK.

[13] Yan, H.S., and Hsieh, L.C., 1994, "Conceptual Design of Gear Differentials for Automotive Vehicles," ASME *Journal of Mechanical Design,* Vol. 116, pp. 565-570.